International Journal of Multiphase Flow 165 (2023) 104486

Contents lists available at ScienceDirect

International Journal of Multiphase Flow

journal homepage: www.elsevier.com/locate/ijmulflow

Effects of SDS surface-active agents on hydrodynamics and oxygen mass transfer in a square bubble column reactor: Experimental and CFD modeling study

Sanaa Kouzbour [a], Francesco Maniscalco [b], Antonio Buffo [b], Marco Vanni [b], Francesc Xavier Grau [c], Bouchaib Gourich [a,*], Youssef Stiriba [c,*]

[a] Laboratoire d'Ingénierie de Procédés et d'Environnement, EST de Casablanca, Oasis Casablanca, BP 8012, Morocco
[b] Department of Applied Science and Technology. Politecnico di Torino, Corso Duca degli Abruzzi 24, 10129, Torino, Italy
[c] ETSEQ, Departament d'Enginyeria Mecanica, Universitat Rovira i Virgili, Av. Països Catalans 26, 43007 Tarragona, Spain

ARTICLE INFO

Keywords:
Bubble column
CFD-PBM coupled model
Surface tension
Bubble size
Gas-liquid mass transfer

ABSTRACT

This work examined experimentally and numerically the effects of sodium dodecyl sulfate (SDS) surfactant agent on mass transfer coefficients k_La_L and k_L in a high-aspect square bubble column reactor. To this end, SDS aqueous solutions at concentrations between 5 ppm and 30 ppm were prepared. Superficial gas velocity was varied from 0.74 cm.s^{-1} to 9.44 cm.s^{-1} covering all flow regimes to analyze the interaction between different phases and the effect of liquid surface tension on gas-liquid interfaces. Experimental data indicated that the presence of the SDS in the liquid phase augmented the overall gas holdup up to 25% at a constant gas velocity ($U_g = 7.3$ cm.s^{-1}) in the transition regime, which is due to the role of SDS in bubble interactions. The impact of SDS addition on the mass transfer is twofold. Firstly, it reduced k_L because the SDS molecules migrate towards the bubble-liquid interface thanks to the lower O_2 diffusivity in water, thus hindering the O_2 transfer from one phase to the other. Secondly, it increased a_L owing to the inhibition of bubbles coalescence and, therefore, the lower mean bubble size. Among these two effects, the latter is prevailing, which led to an increase in k_La_L in contaminated systems. In the second part of this work, a population balance model (PBM) was coupled with a computational fluid dynamics (CFD) model based on large-eddy simulation (LES) to analyze the effect of both tap water and SDS contaminated systems on the breakage phenomena, local flow pattern, and the resulting hydrodynamics and mass transfer features in the reactor. Ultimately, experiments and numerical simulations agreed well in terms of global gas holdup and k_La_L coefficient. In particular, the transition points in the case of the SDS media (except for foam formation) provided the model with adequate PBM definitions for the dispersed phase.

1. Introduction

Bubble column reactors are frequently used in many applications in chemical and biochemical processing industries, environmental processes, and wastewater treatment as multiphase contactors and reactors, owing to the efficient mixing they offer along with a better gas-liquid mass transfer rates and interfacial area with low energy intake (Shah et al., 1982; Shamshirband et al., 2020; Vial et al., 2000; Yang et al., 2011). To improve their design, scale-up, and efficiency and decrease the power consumption of the bioprocess, it is fundamental to understand the relationship between the mass transfer rate and other parameters such as the reactor geometry, operating conditions, and liquid phase properties. The mass transfer performance of bubble columns is extensively linked to the physico-chemical properties of the liquid media and its contained components, and it is influenced by the hydrodynamics in the columns as well as by several multiscale phenomena of gas-liquid flows that occur at the micro/bubble, meso/bubble swarm, and macro/reactor scales (Shiea et al., 2013; Yang et al., 2011). Mass transfer in gas-liquid contactors is usually expressed through the volumetric mass-transfer coefficient k_La_L, where several empirical and/or correlations have been proposed without achieving any degree of generality.

Bubble column-related processes are often associated with the addition or formation of surfactants as impurities, and antifoaming

* Corresponding authors.
E-mail addresses: bouchaib.gourich@univh2c.ma (B. Gourich), youssef.stiriba@urv.cat (Y. Stiriba).

https://doi.org/10.1016/j.ijmultiphaseflow.2023.104486
Received 6 December 2022; Received in revised form 8 April 2023; Accepted 12 April 2023
Available online 13 April 2023

agents in the liquid phase that are used to reduce the negative impact of the foam generated by organic materials and surface-active compounds, or both. For instance, handling emerging contaminants during treatment, such as surfactants, is one of the most prominent and challenging tasks in wastewater biological treatments and environmental processes (Palmer and Hatley, 2018). Indeed, the occurrence of these surface-active agents has a noticeable effect on hydrodynamic and mass transfer characteristics. Surfactants are adsorbed at the interface of the gas-liquid systems, and they reduce the surface tension, as their concentration increases until the critical micelle concentration (CMC) is attained. Moreover, surfactants play a crucial role in the bubble breakage and coalescence phenomena in contaminated systems, since they settle at the bubble-liquid interface and immobilize the interface: the breakage is thereby strengthened and the probability of a successful bubbles collision (*i.e.,* a collision leading to coalescence) is lowered (Falzone et al., 2018). Nevertheless, it is still a complex undertaking to quantify these effects and there is a lack of numerical and experimental research works on the mass transfer in large bubble column reactors at various flow regimes and in the presence of surfactants. Therefore, a brief review of the most relevant studies on the effect of surfactants on hydrodynamics and gas-liquid mass transfer in bubble columns is developed in the following paragraphs.

In light of this, Nekoeian et al. (2021) provided a comprehensive review of recent research on the effects of surfactants, as leading wastewater contaminants, on the mass transfer in bubble columns. They concluded that almost all types of surfactants, anionic, cationic, and nonionic had a favorable effect on gas holdup and specific interface area while negatively influencing bubble size and bubble rise velocity, as reported by Alves et al., (2005) and Clift et al. (2005). Meanwhile, they also listed some references that stated opposite findings and mentioned the need for further investigations to better understand the effects of surfactants on the mass transfer coefficient k_L, and shed light on the reasons behind the discrepancies and sometimes contradictory results. Throughout the literature, it can be noticed that some studies (Alves et al., 2005; Aoki et al., 2015; Cuenot et al., 1997; Dani et al., 2006; Haghnegahdar et al., 2016; Hébrard et al., 2009; Jamnongwong et al., 2010; Lebrun et al., 2022; Takagi and Matsumoto, 2011) studied single contaminated rising bubbles in infinite liquid; whereas other works (Koynov et al., 2006, 2005) showed that the swarm bubble motions are more complex and exhibit different behavior depending on the concentration and bubble size distribution due to the complex bubble-bubble interactions. Therefore, the present work is oriented toward understanding and evaluating the hydrodynamics and mass transfer in two-phase flow systems where a cluster of bubbles are dispersed in the liquid phase with the presence of SDS, which is the most commonly used anionic surfactant.

Several studies on the effects of surfactants on volumetric mass transfer coefficient inside bubble column reactors have been published. For instance, Painmanakul et al. (2005) used a small bubble column with a single orifice to investigate the effect of anionic (SDS) and cationic surfactants (Lauryl dimethyl benzyl ammonium bromine) on mass transfer and revealed that for any surfactant type and concentration, the mass transfer coefficients (k_L and k_La) values were lowest and significantly smaller than those of tap water. Moreover, Sardeing et al. (2006) examined the effect of different surfactant types (anionic, cationic, and non-ionic) on the mass transfer rate of bubbles in a small-scale bubble column. Thus, the obtained results indicated that whatever the liquid phase, three zones are found on the liquid-side mass transfer coefficient variation with the bubble diameter. Asgharpour et al. (2010) evaluated the hydrodynamics, k_La, and Sauter bubble diameter in a bubble column with a height of 1 m and a diameter of 95 mm where the gas was injected through a perforated gas sparger at low superficial gas velocities. They employed three decane chain-containing hydrocarbons and SDS as surfactants and stated that at higher gas velocities a slight addition of alkane led to an increase in k_La and concomitantly to a sharp decrease in Sauter mean bubble diameter. In fact, this effect was attributed to the bubble coalescence inhibition in the presence of contaminant molecules and to the lower surface tension. In hydrocarbon-contaminated solutions, it was observed that k_L diminished as the superficial gas velocity augmented. While the specific transfer area a_L was found to be larger than that of pure water at $U_g \leq 1.5$ cm.s^{-1}. Gómez-Díaz et al. (2009) utilized a 1m high bubble column with an internal diameter of 6 cm equipped with a single orifice as a gas distributor to supply the column with pure carbon dioxide at a low flow rate. The Decyltrimethylammonium bromide (DTABr) as a cationic surfactant was added to analyze its effect on the gas-liquid absorption process. Hence, an increase in the mass transfer coefficient was observed at very low surfactant concentrations and this trend was related to the gas-liquid turbulence in the liquid film, due to the Marangoni effect caused by the surfactant at the aqueous liquid. However, with the presence of Tween 80 as a high-molecular-weight non-cationic surfactant in the same bubble column reactor, García-Abuín et al. (2010) reported that even at low concentration, it had an adverse effect and resulted in a reduction in mass transfer and no influence on gas holdup was noticed. This behavior is therefore assigned to the size of surfactant molecules at the gas-liquid interface. Aubin et al. (2010) and Jia et al. (2015) examined the effect of different cationic surfactants of different chain lengths, molecular sizes, and CMCs on k_L using the same experimental setup to analyze the combined and competitive Marangoni effects caused by the surface tension gradients near the interface and the barriers ones due to the renewal rates around the bubbles. Their conclusions were consistent with those obtained by previous studies that pointed on the dependence of the mass transfer absorption of CO_2 on the nature and concentration of the surfactant. Takagi and Matsumoto (2011) presented a literature review of the bubble behaviors caused by the surfactant adsorption/desorption on the bubble surface. Furthermore, Ahmia et al. (2019) studied the effects of SDS surfactants and microcrystalline cellulose on water system and showed that their combination decreased the mass transfer coefficient. McClure et al. (2015) conducted an experimental and computational study to investigate the influence of 2-propanol addition on the gas holdup, bubble size distribution, and liquid velocity in a 2 m high bubble column with 0.39 m in diameter operating at a superficial gas velocity in the range of 1 – 28 cm. s^{-1}. The findings indicated that the surfactant addition enhanced both local and global gas holdup and increased the mixing time as well. Furthermore, they modified the drag interfacial force in their CFD model to account for the surfactant addition effect and therefore achieve a good agreement with their local measurement. CFD Coupled with the population balance model approach was also tested by Gemello et al. (2019) to validate their experimental data in a bubble column operated in a turbulent churn flow regime considering the impact of different gas spargers along with the presence of different additives in order to address the coalescence and breakup phenomena. Additionally, in our previous research works, the influence of flotation collectors (amine and ester) as cationic and anionic surface-active agents on the hydrodynamics and oxygen mass transfer in 3 m square bubble column equipped with a perforated gas distributor operated at superficial gas velocity varied from 0.97 to 9.44 cm.s^{-1} was investigated. In fact, although both collectors led to a decrease in the k_La_L coefficient, their effects on gas retention as well as the transition velocity were entirely dissimilar.

According to the analysis of the research studies carried out, only a few publications are found that deal with experimental and CFD simulations of surfactant effects on mass transfer performance. Moreover, in most of them, the turbulence is modeled through the traditional Reynolds Averaged Navier- Stokes equation (RANS) approach. Therefore, the present study aims to investigate the global hydrodynamics and mass transfer characteristics experimentally and numerically in a square bubble column reactor operating at both homogenous and turbulent-churn flow regimes with tap water and SDS aqueous solutions as liquid phases. Firstly, the effects of surfactant concentration and superficial gas velocity (U_g) on the overall gas holdup, the flow regime, and the volumetric mass transfer coefficient k_La_L are analyzed. Then,

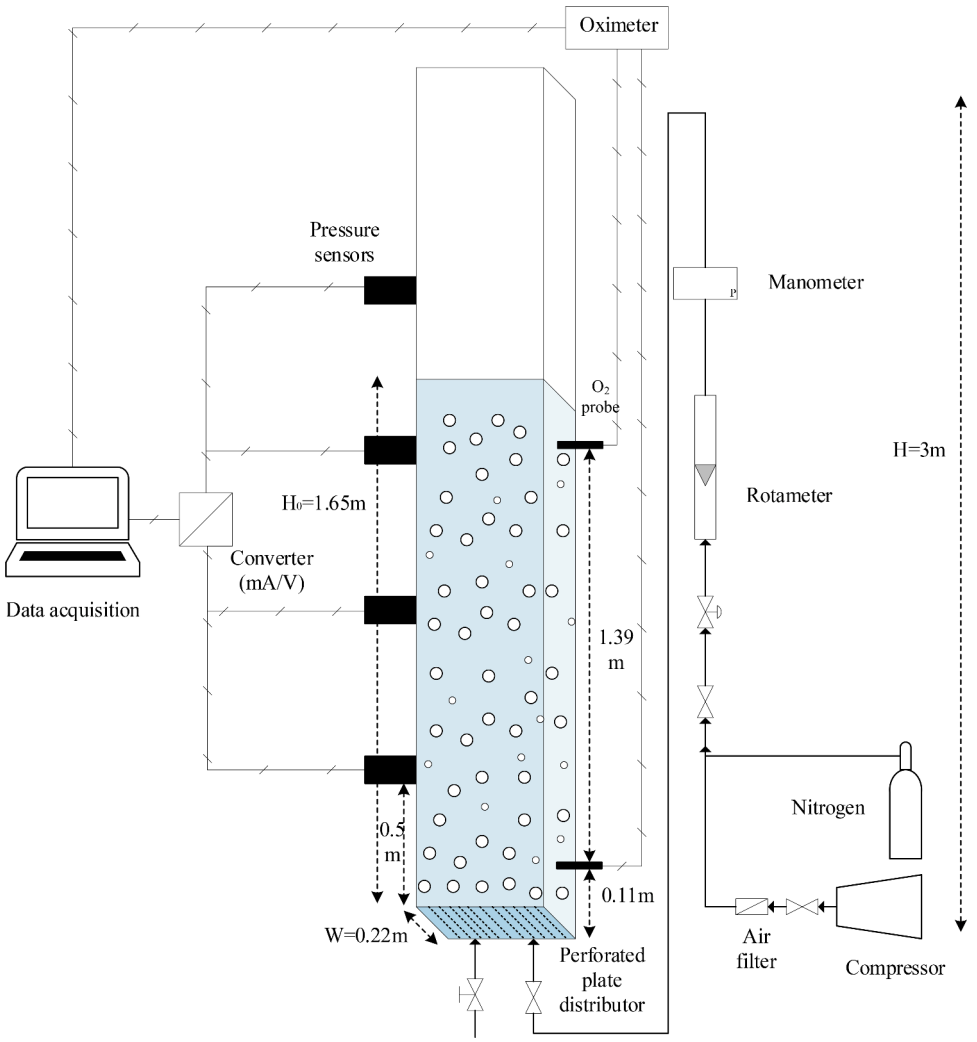

Fig. 1. A schematic diagram of the square bubble column setup (Kouzbour et al., 2021).

Table 1
Physical properties of the liquid phases at 25 ± 2°C.

Medium	Concentration (ppm)	Surface tension (mN m^{-1})	Apparent viscosity (mPa s)
Water	-	72.9 ± 0.9	1.10 ± 0.05
SDS	5	69.2 ± 1.2	1.12 ± 0.02
	10	59.6 ± 0.9	1.14 ± 0.06
	15	51.6 ± 0.2	1.09 ± 0.03
	20	50.1 ± 1.0	1.11 ± 0.12
	30	48.2 ± 1.6	1.08 ± 0.10

three-dimensional Eulerian-Eulerian CFD simulations based on large eddy simulation (LES) are coupled with a Population Balance Model (PBM), where the Quadrature Method of Moments (QMOM) is employed to predict bubble size distribution and analyze breakup and coalescence phenomena. As a matter of fact, the coupling of PBM to LES modeling of turbulence, either in pure or contaminated systems, has not yet been applied to the simulation of complex bubbly flows. Nevertheless, this study proves its successfulness in the prediction of the key design parameters: the overall gas holdup and, above all, the mass transfer coefficient $k_L a_L$. Particularly, the liquid-side mass transfer coefficient k_L is calculated as the ratio of the calculated volumetric mass transfer coefficient and the specific interfacial area. The coupled CFD-PBM is adopted to predict the flow transitions and the resulting changes in local hydrodynamic, flow structure, and mass transfer features.

2. Experimental and numerical methods

2.1. Experimental setup

The experimental setup illustrated in Fig. 1, is a square bubble column made of Plexiglas with dimensions 0.2 m × 0.2 m × 3 m (L×W×H). Compressed air was consistently used as the gas phase and was introduced into the column through a perforated plate with 246 holes of 0.9 mm in diameter located at the bottom of the column, which guarantees uniform aeration. The gas flow rate was controlled using a calibrated rotameter (Brooks Instrument®, GT1000) with a precision of 2%, and the superficial gas velocity ranged from 0.75 to 9.44 cm s^{-1}. The liquid phase was fed into the column through a valve placed at the bottom of the column. The liquid phase was operated in a batch mode and the clear liquid height H_0 was adjusted to 1.65 m. All experiments were performed at ambient temperature and atmospheric pressure.

2.2. Surfactant aqueous solutions, preparation, and characterization

The Sodium Dodecyl Sulfate (SDS), which is a commercial collector purchased from Merck (Germany), was used as an anionic surfactant and added to the liquid phase (tap water). The SDS is largely employed for the treatment of heavy metals from wastewater (Salmani et al., 2013). The studied concentrations ranged from 5 to 30 ppm, as previously performed by Kouzbour et al. (2021), to compare the outcome with other cationic and anionic surfactants and to minimize foaming. All

surfactant solutions were prepared by adding the SDS collector to tap water and subsequently stirring for 10 – 15 min at a temperature of 25°C. Experiments were also repeated with tap water as the reference fluid. The surface tension of each solution was measured using a Krüss tensiometer (K12-Krüss©, Germany) and the Wilhelmy plate method with an accuracy of ± 1 mN.m^{-1}. The surface tension of tap water and aqueous solutions in different concentrations are summarized in Table 1. From this table, it can be deduced that the critical micelle concentration (CMC), which corresponds to a saturated interface, is achieved when SDS content is about 15 ppm. The rheological studies of the solutions were carried out using an AR-G2 rheometer (TA Instruments, USA) with a 40 mm $-$ 2° steel cone geometry. A simple shear study with a shear rate ranging from 1 to 1000 s^{-1} was performed to determine the apparent viscosity value at 25°C. The measured apparent viscosity of the solutions is represented in Table 1.

2.3. Measuring techniques in bubble column

2.3.1. Gas holdup measurements

The overall gas holdup in the column was measured using the manometric method. Neglecting the acceleration and wall friction contribution in the momentum balance and considering $\rho_G \ll \rho_L$, the gas holdup can be deduced by the following expression:

$$\varepsilon_g = 1 - \frac{\Delta P}{\rho_L g \Delta H} \tag{1}$$

where ΔP is the difference of static pressure between two sensors placed at a distance ΔH. Pressure measurements were performed using four piezo-resistive sensors embedded in the wall (Keller PR-25/8797.1), with respective pressure ranges 0 $-$ 500 mbar (for the two lowest sensors), 0 $-$ 150 mbar (for the two top sensors), with an accuracy of 0.02% of the full scale. The distance between the pressure sensors was 0.5 m (from 0.5 m to 2 m above the gas sparger). Pressure signals were sampled with a 16-bit acquisition card (Adlink-1901, *Adlink Technology Inc.*, Taiwan) and stored in a PC. The *Adlink®Utest* software was employed to control data acquisition. Pressure signals were sampled with a frequency of 100 Hz and a duration of 200 s. Thus, the acquisition length was 20,000 points for each experiment. Three samples for each condition were conducted to diminish statistical error.

2.3.2. Volumetric mass transfer coefficient measurements

The volumetric mass transfer coefficient $k_L a_L$ was measured using the dynamic deoxygenation method (Gourich et al., 2008), which is based on oxygen elimination by bubbling nitrogen followed by reoxygenation using compressed air. In the batch liquid phase, the variation of dissolved oxygen concentration with time is measured using two dissolved oxygen electrodes (WTW Cellox 325) located at 0.11 m and 1.50 m above the perforated plate. These are connected to a DO-meter (WTW OXI 197i) and a data acquisition system (Adlink-1901) allowing the recording of concentration values. It is worth noting that the oxygen probes are immersed to a depth of 9 cm. A mass balance on dissolved oxygen (and assuming a perfectly stirred bubble column) gives:

$$\frac{dC_t}{dt} = k_L a_L (C_s - C_t) \tag{2}$$

where C_s is the dissolved oxygen concentration at saturation and C_t is the instantaneous dissolved oxygen concentration measured by experiments. Integrating Eq. (2) we get:

$$\ln \frac{C_s - C_0}{C_s - C_t} = k_L a_L t \tag{3}$$

where C_s is the initial dissolved oxygen concentration. The value of $k_L a_L$ is obtained from the slope of the curve of $\ln \frac{C_s - C_0}{C_s - C_t}$ versus t.

The volumetric oxygen transfer coefficients measured at the temperature T ($k_L a_{L_T}$) are then reported at 20°C ($k_L a_{L_{20}}$) using the following temperature correction:

$$k_L a_{L_{20}} = k_L a_{L_T} \times \theta^{(20-T)} \quad \text{with } \theta = 1.024 \tag{4}$$

Bubble size was measured using image analysis. Pictures of the bubbly flow were taken and analyzed using the free ImageJ software. However, this technique was limited to low gas holdup, due to the influence of light obstruction by the bubbles on flow imaging.

2.4. Computational modeling and setup

2.4.1. Flow equations

The Eulerian-Eulerian framework is adopted to model the local hydrodynamics of the gas-liquid two-phase flow system. The filtered mass and momentum conservation equations are solved for each phase k and given by:

$$\frac{\partial(\alpha_k \rho_k)}{\partial t} + \nabla\cdot(\alpha_k \rho_k \mathbf{u}_k) = 0 \quad (k = \text{ liquid or gas}) \tag{5}$$

$$\frac{\partial(\alpha_k \rho_k \mathbf{u}_k)}{\partial t} + \nabla\cdot(\alpha_k \rho_k \mathbf{u}_k \mathbf{u}_k) = -\alpha_k \nabla p + \alpha_k \rho_k \mathbf{g} + \nabla\cdot(\alpha_k \rho_k \boldsymbol{\tau}_k) + \mathbf{F}_k \tag{6}$$

where α_k is the phase fraction, ρ_k is the density, $\mathbf{u}_k$ is the resolved (filtered) velocity, and $\boldsymbol{\tau}_k$ is the subgrid-scale (SGS) stress tensor of phase k defined as:

$$\boldsymbol{\tau}_k = -\mu_{\text{eff},k}\left(\nabla \mathbf{u}_k + (\nabla \mathbf{u}_k)^T - \frac{2}{3} I (\nabla\cdot \mathbf{u}_k)\right) \tag{7}$$

where $\mu_{\text{eff},k}$ is the effective viscosity. This term represents the unknown part of the sub-grid scale models in the LES and following the work of Sato and Sekoguchi (1975), the effective viscosity in the liquid phase is assumed to be composed of three contributions; the molecular viscosity, the shear-induced turbulent viscosity, and the bubble induced turbulence viscosity.

$$\mu_{\text{eff},k} = \mu_{L,L} + \mu_{SGS,L} + \mu_{BIT,L} \tag{8}$$

The last term of the right-hand side of Eq. (6), $\mathbf{F}_k$, is the interfacial force exchange between the two phases accounting for the virtual mass, drag, and lift among others, and p is the pressure. Although the relevance of each interfacial force and the closure to be applied is still under debate (Muniz and Sommerfeld, 2020), no consensus has been achieved yet. It was shown that the implementation of the drag force, $\mathbf{F}_D$, with the correction accounting for the bubble swarms led to reliable results, especially at high gas velocity (Gemello et al., 2018; Maniscalco et al., 2021):

$$\mathbf{F}_D = \frac{3}{4} h \, C_D^{\infty} \frac{\rho_L \alpha_G}{d_b} \, |\mathbf{u}_r| \mathbf{u}_r \tag{9}$$

Here $\mathbf{u}_r = \mathbf{u}_G - \mathbf{u}_L$ is the relative velocity and the drag coefficient for an isolated bubble C_D^{∞} is calculated using the correlation proposed by Tomiyama (1998) for partially contaminated air-water systems:

$$C_D^{\infty} = \max\left[\min\left(\frac{24}{Re_b}\left(1 + 0.15 Re_b^{0.687}\right), \frac{72}{Eo_b}\right), \frac{8}{3}\frac{Eo_b}{4 + Eo_b}\right] \tag{10}$$

and then adjusted by multiplying it by the swarm factor h to take into account the presence of a plurality of bubbles close to each other (Simonnet et al., 2008):

$$h = (1 - \alpha_G)\left[(1 - \alpha_G)^{25} + \left(4.8 \frac{\alpha_G}{1 - \alpha_G}\right)^{25}\right]^{-2/25} \tag{11}$$

However, it could be pointed out that, in the systems investigated in this study, the sole use of Eq. (10) for the calculation of the drag coefficient may not be sufficiently accurate, since the air-SDS system can be

considered rather as totally than partially contaminated systems and, therefore, Eq. (10) could lead erroneous calculation of the drag force. As discussed further, the main effect of the addition of SDS to an air-water system is the immobilization of the bubble's interface and consequently the increase in drag force and decrease in bubble terminal velocity. Nevertheless, Tomiyama et al. (1998) showed that this effect is relevant only for bubbles with a diameter lower than 3 mm and thus does not concern the present work which focuses on systems with larger bubble sizes. In the latter case, the drag coefficients for partially and fully contaminated systems are identical. On this basis, only the drag coefficient for partially contaminated systems was used.

The effect of the other interfacial forces was tested in this study. Specifically, the effective impact of the lift force associated with the presence of a velocity gradient in the liquid phase close to the bubble inducing its lateral motion, and that of the turbulent dispersion force which results from the turbulent eddies of the liquid phase, were assessed for different superficial gas velocities. Indeed, simulations performed including the lift force using the lift coefficient; proposed by Tomiyama et al. (2002); particularly exhibited unrealistic results that probably originated from numerical instabilities. In contrast, according to Lopez de Bertodano et al. (1994), the inclusion of the turbulent dissipation force modeled using $C_{TD} = 0.6$ (Fard et al., 2020a) did not bring any significant difference in the overall gas holdup and k_La_L coefficient results. Also, the same authors (Fard et al., 2020a, 2020b) highlighted the importance of this interfacial force in simulating both the local liquid axial velocity and the gas holdup at high superficial gas velocities corresponding to churn-turbulent flow regimes. It is noteworthy that readers are recommended to consult the reference (Fard et al., 2020a) where the adopted expressions for these interfacial forces are provided.

As aforementioned, most studies concerning the simulation in bubble columns opted for a RANS description of the turbulence as it represents the simplest and the most assessed modeling at the industrial scale. However, Fard et al. (2020a) and Maniscalco et al. (2021) recently showed that the LES model can be also applied with an affordable computational demand. Therefore, the turbulence effects were modeled for the continuous (liquid) phase using LES which, as previously discussed, directly resolves the scales of motion larger than a certain cut-off length Δ, whereas the scales smaller than Δ (or subgrid-scale, SGS) are modeled through the computation of the SGS turbulent viscosity μ_{SGS}. In this work, Smagorinsky model (Smagorinsky, 1963) was employed to calculate the turbulence of the liquid phase:

$$\mu_{L,t} = \mu_{L,SGS} = \rho_L(C_s\Delta)^2|\mathbf{S}_L| \tag{12}$$

with the addition of the bubble-induced turbulence (BIT) viscosity to take into account the contribution of the bubble motion to the liquid turbulence as per Zhang et al. (2006):

$$\mu_{L,t} = \mu_{L,SGS} + \mu_{L,BIT} = \rho_L(C_s\Delta)^2|\mathbf{S}_L| + \rho_L C_{\mu,BIT}\alpha_G|\mathbf{u}_r| \tag{13}$$

Eventually, the SGS and BIT viscosities are added up to the laminar viscosity as shown in Eq. (8). Here C_s and $C_{\mu,BIT}$ are model constants, which are respectively equal to 0.1 and 0.6. Δ is the cut-off filter set equal to the cell size ($\Delta = \sqrt[3]{\delta x\delta y\delta z}$) and $\mathbf{S}_L$ is the liquid phase strain rate. The gas phase has a sensible lower density than the liquid phase and hence it is treated like a laminar flow phase.

The principal drawback of the Eulerian-Eulerian approach is that the bubble size must be fixed as constant. This assumption may be unrealistic when break-up and coalescence phenomena occur due to bubble-bubble and bubble-liquid interactions in transition or churn-turbulent flow regimes, leading to a variable bubble size distribution. That is why the coupled CFD-PBM can be seen as an alternative to overcome this limitation in Eulerian-Eulerian based methods, where the additional transport equation of the bubble number-density function (NDF), $n(\mathbf{x};L)$ is also solved to properly model the evolution of the bubble size variation present in the flow. Assuming that the NDF depends only on the bubble size (univariate conditions) as an internal coordinate, the additional transport equation to predict the number density of different bubble classes is given by:

$$\frac{\partial}{\partial t}(\rho_G n) + \nabla\cdot(\rho_G n\mathbf{u}_G) = S \tag{14}$$

with S being the source term that accounts for the bubble's birth and death phenomena due to coalescence and break-up. In this study, Eq. (14) is solved through the Method of Moments (Marchisio et al., 2003a), which solves the low-order moments transport equation of the NDF, and the closure problem is solved using the Quadrature Method of Moments (QMOM) (Marchisio et al., 2003b). This method calculates the k-order moment of the NDF, m_k, using a quadrature approximation:

$$m_k = \int_0^{+\infty} n(L)L^k dL \approx \sum_{i=1}^{N} w_i L_i^k \tag{15}$$

The moments of the NDF are not only mathematical entities but they are connected to physical quantities of the system: the moment of order 2 and 3 are respectively connected to the interfacial area and the volume of the bubbles through the area shape factor k_a and the volumetric shape factor k_v. In this way, it is possible to estimate the Sauter mean diameter d_{32} as the ratio of these two moments:

$$d_{32} = m_3/m_2 \tag{16}$$

The source term for the moment of order k is computed as follows:

$$S_k = \frac{1}{2}\sum_{i=1}^{N} w_i \sum_{j=1}^{N} w_j h(L_i,L_j)\left[\left(L_i^3 + L_j^3\right)^{\frac{k}{3}} - L_i^k - L_j^k\right] + \sum_{i=1}^{N} w_j g(L_i)\left(\overline{b}_i^k - L_i^k\right) \tag{17}$$

where w and L are respectively the quadrature weights and abscissas. While $h(L_i,L_j)$, $g(L_i)$ and $\overline{b}_i^k$ are the coalescence kernel, the breakage kernel, and the k-order moment of the daughter size distribution $\beta(L,L_i)$, respectively:

$$\overline{b}_i^k = \int_0^{L_i} \beta(L,\ L_i)L^k dL \tag{18}$$

The coalescence kernel, $h(L_i,L_j)$, is composed of collision frequency $h_0(L_i,L_j)$ and collision efficacy $\eta(L_i,L_j)$:

$$h(L_i,L_j) = h_0(L_i,L_j)\ \eta(L_i,L_j) \tag{19}$$

In the last decades, several approaches have been studied and developed for the estimation of Eq. (19) including contaminated systems as investigated in the work of Falzone et al. (2018). In the studied system, collisions are mainly resulted from turbulent fluctuations where bubbles are continuously hit by turbulent eddies belonging to the inertial subrange that cause the bubble's chaotic motion, eventually leading to a collision. According to Coulaloglou and Tavlarides (1977), the collision frequency can be written as:

$$h_0(L_i,L_j) = C_1\epsilon_L^{\frac{1}{3}}(L_i+L_j)^2\sqrt[2]{L_i^{2/3}+L_j^{2/3}} \tag{20}$$

with $C_1 = 0.28$ and the liquid turbulent dissipation rate ϵ_L is estimated by:

$$\epsilon_L = 2\nu_{L,eff}\mathbf{S}_L : \mathbf{S}_L \tag{21}$$

However, a bubbles collision does not always lead to their aggregation and the success of the collisions is linked to the collision efficiency $\eta(L_i,L_j)$. Three main phenomena have been proposed for the derivation of $\eta(L_i,L_j)$ namely the energy model (Sovová, 1981), the critical approach velocity model (Lehr et al., 2002), and the film drainage model (Coulaloglou and Tavlarides, 1977), and were adopted

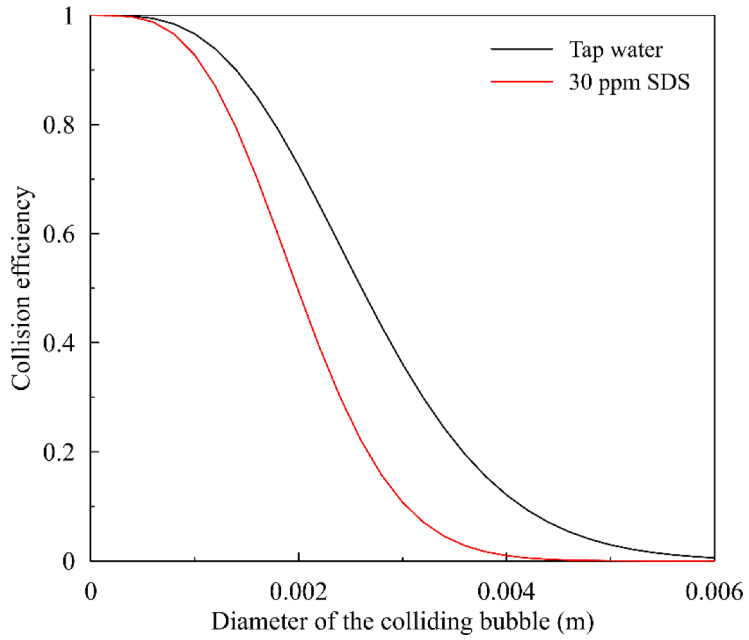

Fig. 2. Collision efficiency for a first bubble hitting a second bubble with a diameter equal to 6 mm as a function of the first bubble size.

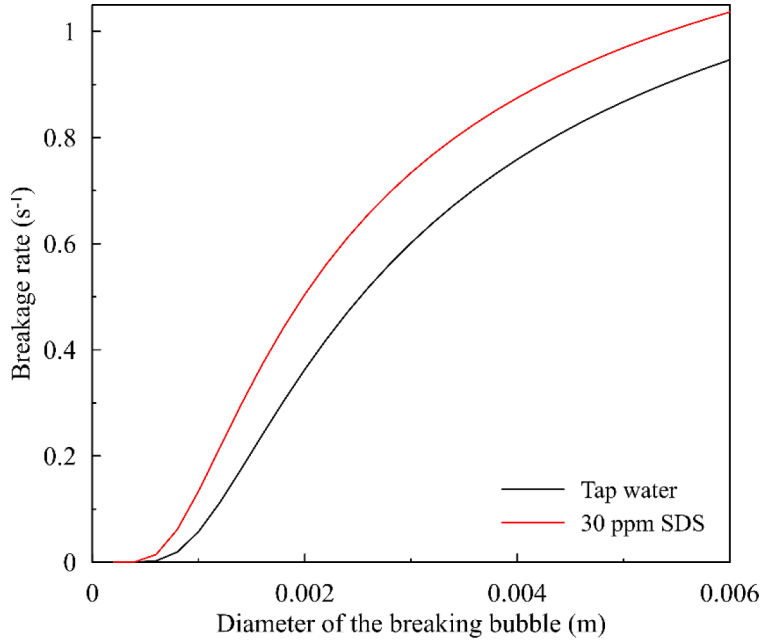

Fig. 3. Breakage rate as a function of the bubble size for tap water and contaminated systems.

in this study. According to the latter, the collision efficacy is related to the ratio of the drainage time of the film liquid trapped between the bubbles and the contact time: if the latter is greater than the former, the collision is successful and coalescence occurs:

$$\eta(L_i,L_j)=\exp\left(-\frac{t_{drain}}{t_{cont}}\right)=\exp\left[-C_2\frac{\mu_L\rho_L\epsilon_L}{\sigma^2}\left(\frac{L_iL_j}{L_i+L_j}\right)^4\right] \quad \text{with } C_2=6.0\times10^9 \tag{22}$$

On the other hand, the breakage phenomenon differs from the coalescence because it involves only one bubble. In general, it is assumed that turbulent eddies of size comparable to the bubble induce (through the velocity fluctuations) its deformation, elongation, and ultimately when these stresses exceed the interfacial and internal viscous stresses, its break-up. This mechanism caused by turbulent fluctuations is the most adopted to describe bubble breakage in the bubble column. Actually, the expression proposed by Laakkonen et al. (2006) was used in this study:

$$g(L)=C_6\epsilon_L^{1/3}\mathrm{erfc}\left[\sqrt{C_7\frac{\sigma}{\rho_L\epsilon^{2/3}L_i^{5/3}}+C_8\frac{\mu_G}{\sqrt{\rho_L\rho_D}\epsilon^{1/3}L_i^{4/3}}}\right] \tag{23}$$

where C_6, C_7 and C_8 are model constants. Moreover, the break-up of a bubble implies the birth of two or more daughter bubbles, whose size needs to be evaluated. To this end, a daughter size distribution function (DSD) must be specified. Indeed, three different types of DSD functions

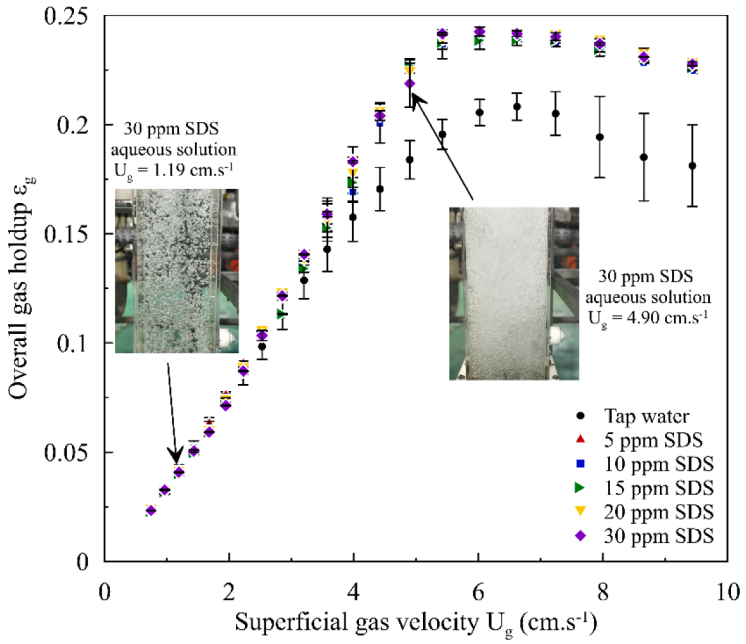

Fig. 4. Overall gas holdup versus superficial gas velocity for air−SDS aqueous solutions.

are found in the literature, which are empirical, phenomenological, and statistical functions. Besides, the function proposed by Laakkonen et al. (2007) and (2006) belongs to the latter type and it is modeled as a beta-function assuming binary breakage:

$$\beta(L,L_i) = 180\left(\frac{L^2}{L_i^3}\right)\left(\frac{L^3}{L_i^3}\right)^2\left(1-\frac{L^3}{L_i^3}\right)^2 \tag{24}$$

The presence of contaminants such as surfactants and salts may play a non-negligible role in the breakage and coalescence phenomena. Therefore, their occurrence should be considered in the respective kernels. Typically, the presence of surfactants improves breakage by reducing the interfacial tension and the partial immobilization of the bubble interface and inhibits coalescence because the surfactant molecules accumulate at the gas-liquid interface, introducing an extra repulsive force term between bubbles that impedes coalescence phenomenon. Moreover, a gradient of surfactant molecules concentration on the interface is responsible for a surface tension gradient and, thus, Gibbs-Marangoni effects that increase the film drainage time (Falzone et al., 2018). However, when the surfactant concentration is low, as is the case for the systems investigated in the present work, the impact on the bubble break-up and coalescence can be modeled by simply updating the interface tension. This strong assumption is supported by the satisfactory results (section 3.1) provided using the drag coefficient for both air-water and air-SDS aqueous solution systems and was previously justified.

Since, with these bubble dimensions, the fluid dynamics is not significantly affected by the presence of the SDS molecules, it can be assumed that the resulting immobilization of the interface does not play a considerable role in either bubbles coalescence or breakage and these events are more largely affected by the reduced surface tension. Therefore, in the PBM equations, the regular kernel was used to account for bubble coalescence and breakage, considering only the decrease of the interfacial tension and not the interface immobilization. Despite this simplification, it should be pointed out that the accuracy and the quality of the CFD results are remarkable, as shown by the estimation of the gas-liquid mass transfer coefficients (Section 3.3).

In this work, coalescence is considered by including the collision frequency due to turbulent fluctuations (Eq. (20)) and the efficiency related to the film drainage time (Eq. (22)), while the breakage is modeled by adopting the turbulent fluctuations approach (Eq. (23)) coupled with DSD as expressed by Eq. (24).

Finally, to further strengthen the above-stated hypothesis, a comparison between collision efficiency (Eq. (22)) and breakage frequency (Eq. (23)) is performed to evaluate the impact of the interfacial tension change. These expressions were explicitly chosen for this comparison since the interfacial tension is present in both. The analysis is carried out keeping constant all the quantities except for the bubble size (or in the case of the collision efficiency of one of the colliding bubbles): in particular, a value of 0.05 m^2.s^{-3} is considered for the turbulent dissipation rate and in the Eq. (19), the diameter of the second colliding bubbles is set to 6 mm. Hence, the findings are represented in Figs. 2 and 3 and solidly support what was previously stated: the presence of the surfactant obtained from varying the interfacial tension of the two-phase systems induces a smaller bubble size owing to a lower coalescence efficiency and a higher breakage rate.

2.4.2. *Mass transfer coefficient and interfacial area estimation*

With the CFD simulation, the oxygen mass transfer coefficient was estimated using the approach proposed by Lamont and Scott (1970), which is based on the penetration theory as first proposed by Higbie (1935) and the surface renewal by Danckwerts (1951). According to this approach, the mass transfer coefficient k_L depends on the time that turbulent eddies spend close to the interface and their exposure renewal period, which is affected by the turbulent motion ranging from the Kolmogorov range to the inertial range:

$$k_L = C_k\sqrt{D_{O_2}\sqrt{\frac{\epsilon_L}{\nu_L}}} \tag{25}$$

with D_{O_2} is the oxygen diffusivity coefficient, ν_L the liquid laminar kinematic viscosity, and C_k a model constant equal to 0.4. It is important to point out that the presence of surfactants has a non-negligible impact on D_{O_2}, since they accumulate at the gas-liquid interface hindering mass transfer. Hence, D_{O_2} decreases as the surfactant concentration increases and the D_{O_2} values used in this work (for the SDS-contaminated systems) were extrapolated from the investigation conducted by Hébrard et al. (2009). Meanwhile, the specific interfacial area a_L, as mentioned in Sub-section 2.4.1, is directly linked to the 2-order moment through the area shape factor $k_a = \pi$ and it can be easily computed as:

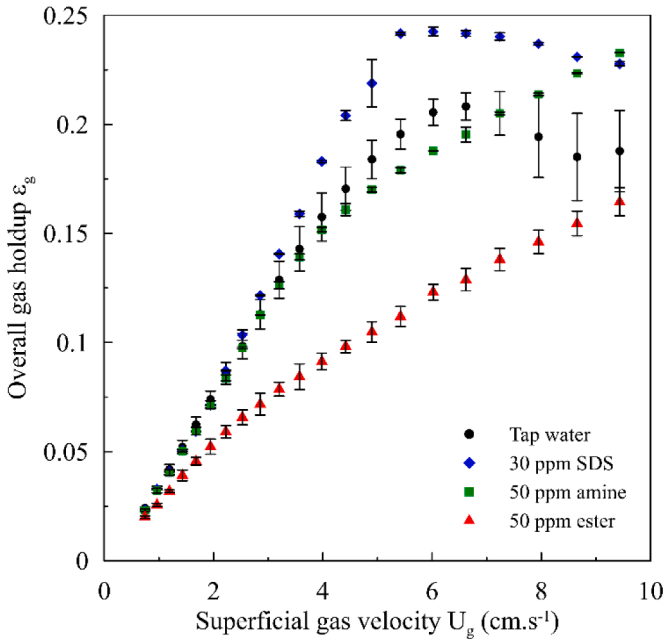

Fig. 5. The effect of different surfactants on overall gas holdup measurements (adapted from Kouzbour et al. (2021)).

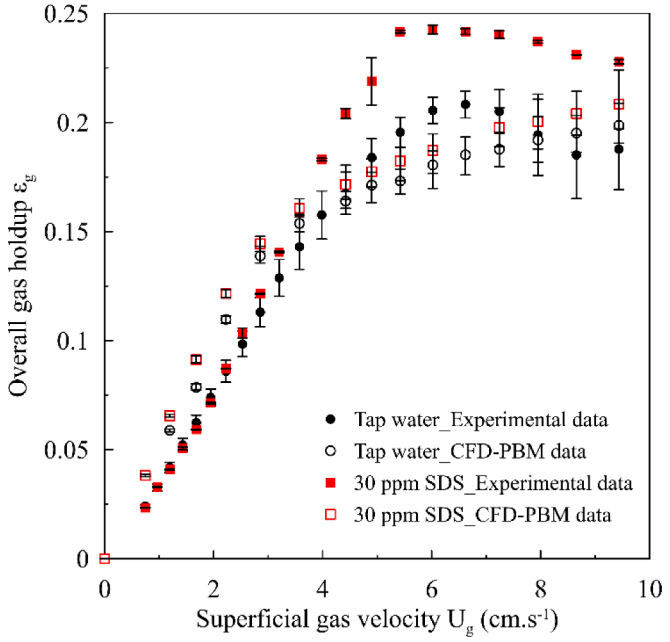

Fig. 6. Comparison of the overall gas holdup obtained through CFD-PBM simulation with experimental ε_g measurements.

$$a_L = \pi m_2 \tag{26}$$

2.4.3. Computational setup

Simulations were performed using the twoPhaseEulerFoam solver in OpenFOAM 5. The average cell size of the mesh was set according to the criterion proposed by Milelli et al. (2001). Simulations were transiently run for a total simulated time equal to 100 s with a time step chosen so that the Courant number was always smaller than 0.65. The sampling was performed by averaging the last 60 s of simulations and after discarding the initial 40 s in order to discard the behavior biased by the initial conditions and to allow the settlements of the flow. For the simulations conducted with a fixed diameter, the latter was determined based on the experimental data. The inlet air fraction was set to 0.5, and the air inlet velocity was fixed accordingly to the superficial velocity, while the liquid velocity was set to 0. At the walls, a no-slip condition for the water velocity and a slip condition for the air velocity were imposed. At the outlet, the boundary conditions for both velocities were set to pressureInletOutletVelocity, while, in the case of backflow, the air fraction was set to 1. In the coupled CFD-PBM simulations, the transport equations for the first six moments were solved, and the three nodes and three abscissas requested for the quadrature approximation were calculated using the Wheeler algorithm (Wheeler, 1974). In the inlet section, the moments were computed by assuming a log-normal distribution centered on the mean Sauter diameter, which was evaluated from experimental measurements with a standard deviation equal to 0.15.

The Van Leer limiter-based scheme was used for spatial discretization for all variables and the Crank-Nicolson scheme was employed for the time discretization.

3. Results and discussion

The section below describes and analyses the achieved experimental and numerical outcomes. Firstly, the overall gas holdup and the two-phase flow characteristics are presented with a particular emphasis on the SDS surfactant addition effects on hydrodynamics and oxygen mass transfer in the bubble column reactor. Next, these findings were compared to the ones of the air-water system. Finally, the results were employed to validate the CFD model. Actually, Local gas holdup, axial liquid velocities, bubble size distributions, and flow patterns were exhibited and discussed. Then, the volumetric mass-transfer coefficient $k_L a_L$ and the liquid-side mass transfer coefficients k_L were estimated.

3.1. Global and local hydrodynamics

The experimental overall gas holdup for tap water and surfactant aqueous solutions as a function of superficial gas velocity is reported in Fig. 4. Regarding the air-water system, the gas holdup increases quasi-linearly for both homogeneous and transition flow regimes, which is mainly attributed to the increase in the bubbles in the liquid phase with the inlet superficial gas velocity, to the coalescence that occurs in the core region of the reactor, and to the type of gas distributor which generates gas bubble of nearly 1 mm diameter. Whereas, in the heterogeneous flow regimes, the overall gas holdup diminishes due to the formation of large bubbles that rise more rapidly than small bubbles. For further details on the global hydrodynamics and flow regime transition for the air-water system, the reader is pointed to the reference (Kouzbour et al., 2021). Henceforth, the focus of our analysis will shift to the effects of the SDS surfactant on global and local hydrodynamics.

As described above, the gas holdup augments quasi-linearly in the homogeneous flow regime ($U_g \leq 3$ cm.s^{-1}) as does the number of small bubbles with the rise of U_g independently of the liquid phase. However, slight changes in ε_g are observed at $U_g = 3$ cm.s^{-1} after the addition of SDS concentrations ranging from 20 to 30 ppm. Indeed, at higher U_g values, the effect of SDS addition on ε_g becomes much more pronounced with a sharper change in the slope at approximately $U_g = 7$ cm.s^{-1} followed by an almost constant value of ε_g. Therefore, the influence of SDS concentrations remains insignificant. According to the surface tension measurements given in Table 1, the augmentation of the SDS surfactant concentration, even though insignificant, induces a decrease in the surface tension, which leads to smaller bubbles with lower rise velocity and subsequently enhances the overall gas holdup. At U_g lower than 3 cm.s^{-1}, the homogeneous flow regime is established, and the sparger generates smaller bubbles with almost preserved size in the column since coalescence phenomena are inhibited as can be seen in the photographic measurements (Fig. 4). This means that the primary bubble size generated by the present gas distributor is similar for both systems. Similar conclusions were also reported by (Asgharpour et al.,

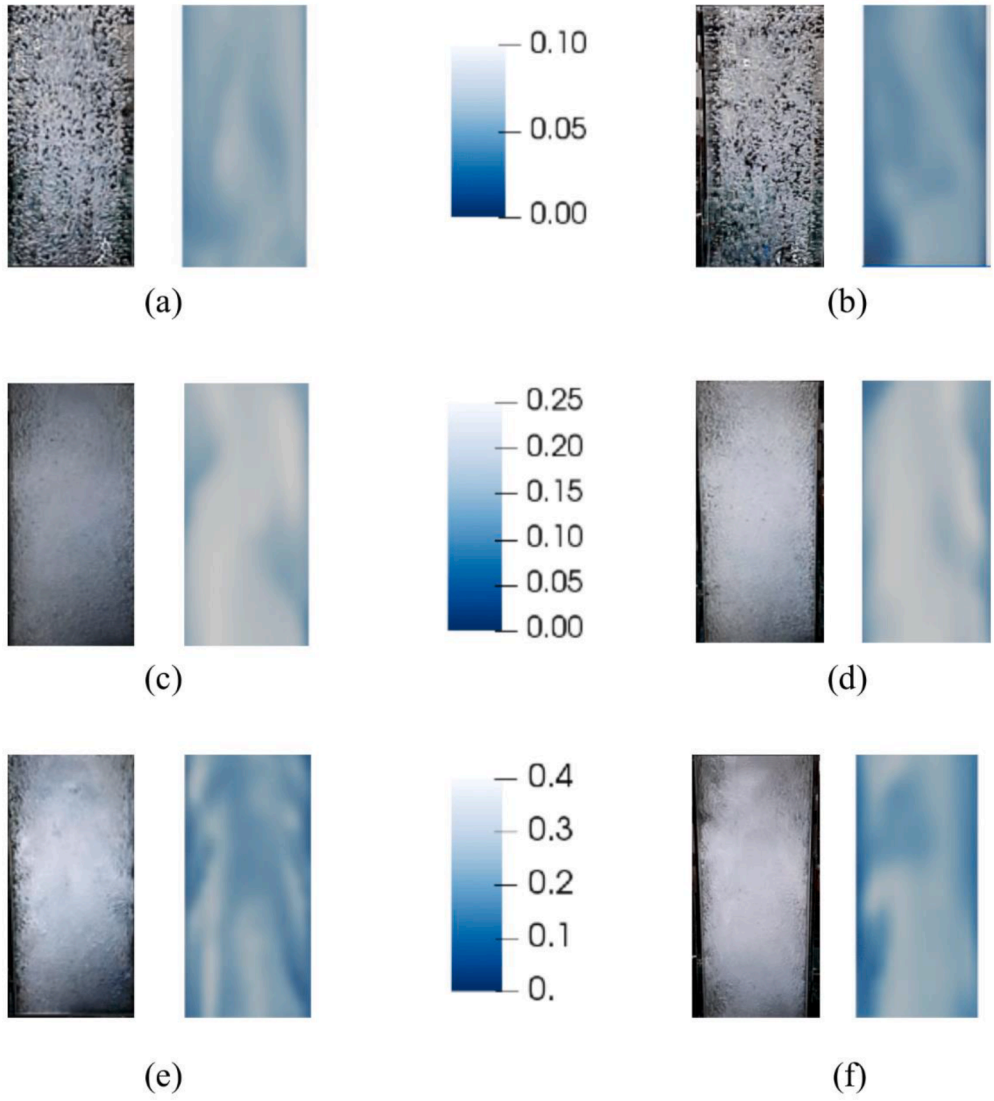

Fig. 7. Comparison of experimental flow patterns and instantaneous contour plot obtained from the volume gas fraction obtained with CFD-PBM simulations at $U_g =$ 1.19 cm.s^{-1} for (a) and (b), $U_g = 4.90$ cm.s^{-1} for (c) and (d), and $U_g = 7.95$ cm.s^{-1} for (e) and (f). Left side pictures ((a), (c), and (e)) represent the configuration with 30 ppm SDS aqueous solution, while right side pictures ((b), (d), and (f)) represent the air-water system.

2010) that employed the same surfactant and a different gas sparger. In fact, such bubbles are always smaller than the bubble size dictated by the surface tension, which implies that further addition of SDS does not affect the gas holdup.

For the same interval of superficial gas velocity, Fig. 5 compares different surfactants already analyzed in our recent works (Kouzbour et al., 2021) and (Ziaei-Halimejani et al., 2021). This figure exhibits that the addition of SDS to water results in a higher overall gas holdup compared to the other surface-active agents. Therefore, this increase could be a consequence of the fact that bubble coalescence is hampered in the SDS aqueous solution (Figs. 4 and 6). In contrast, the overall gas holdup of ester aqueous solutions is significantly lower compared to the tap water, and this was attributable to bubble coalescence which was rapidly initiated (at U_g= 2.9 cm s^{-1} in the case of 50 ppm ester aqueous solution). Meanwhile, for amine aqueous solution, the overall gas holdup is approximately equal to the values reported for the tap water at low superficial gas velocities, but it tends to increase when U_g is greater than 7.3 cm s^{-1} (Fig. 5). In fact, the reason of the ε_g increase is the formation of foam with a height of about 15 – 18 cm at high superficial gas velocities ($\geq$ 7.3 cm s^{-1}). According to Besagni et al. (2019), the formation of a thick cap impedes air disengagement and eventually induces an accumulation of bubbles, thereby significant enhancement of ε_g. In parallel, the evolution of gas holdup in SDS aqueous solution was also accompanied by a foam formation from low U_g; however, the foaming properties are related to the length of the hydrocarbon chain of this surfactant.

Fig. 4 also illustrates that at higher superficial gas velocity, the gas holdup displays a maximum of nearly 0.25 at U_g = 7.3 cm.s^{-1}, which reflects the delay in the transition between homogenous and churn-turbulent flow regimes due to the lower coalescence rate, and then it exhibits a stagnation that entails a plateau similar to what was observed in the case of tap water. This step is characterized by the presence of large bubbles rising through the center of the column at high velocity and contributes weakly to the increase in ε_g. In fact, it is noteworthy that such an increase was significant in the case of amine and ester aqueous solutions as can be noticed in Fig. 5. For air-SDS aqueous solution, the linearity of the global gas holdup curve indicates that the homogeneous flow regime prevails at U_g less 5.5 cm.s^{-1}. Beyond this value, there is a change in the slope followed by a plateau-like zone of the heterogeneous regime. Based on the flow transition analysis of the air-water system reported by Kouzbour et al. (2021), the transition flow regime starts at U_g = 3 cm.s^{-1} with the production of the first coalescence-induced

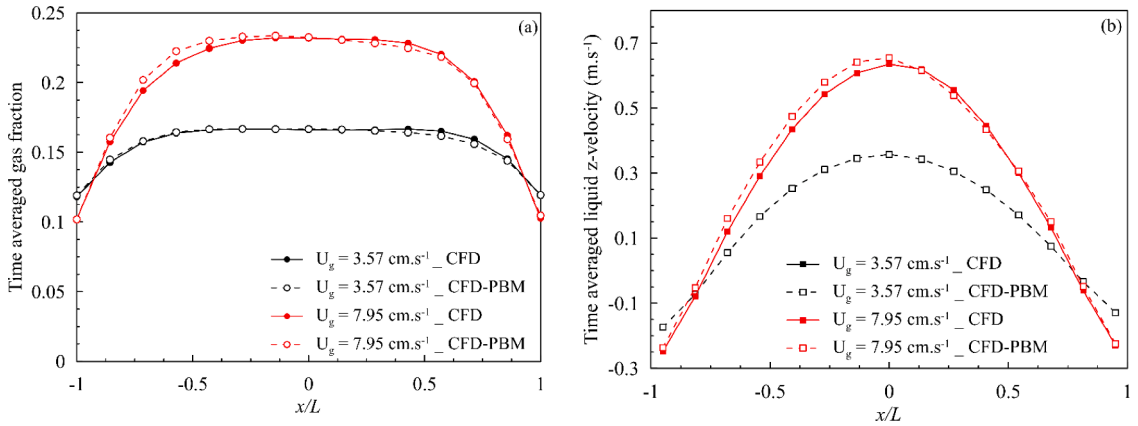

Fig. 8. Impact of population balance modeling. (a) Time-averaged gas fraction and (b) liquid axial velocity radial profiles obtained with CFD simulations for the configuration with tap water at U_g = 3.57 and 7.95 cm.s^{-1} with and without population balance modeling.

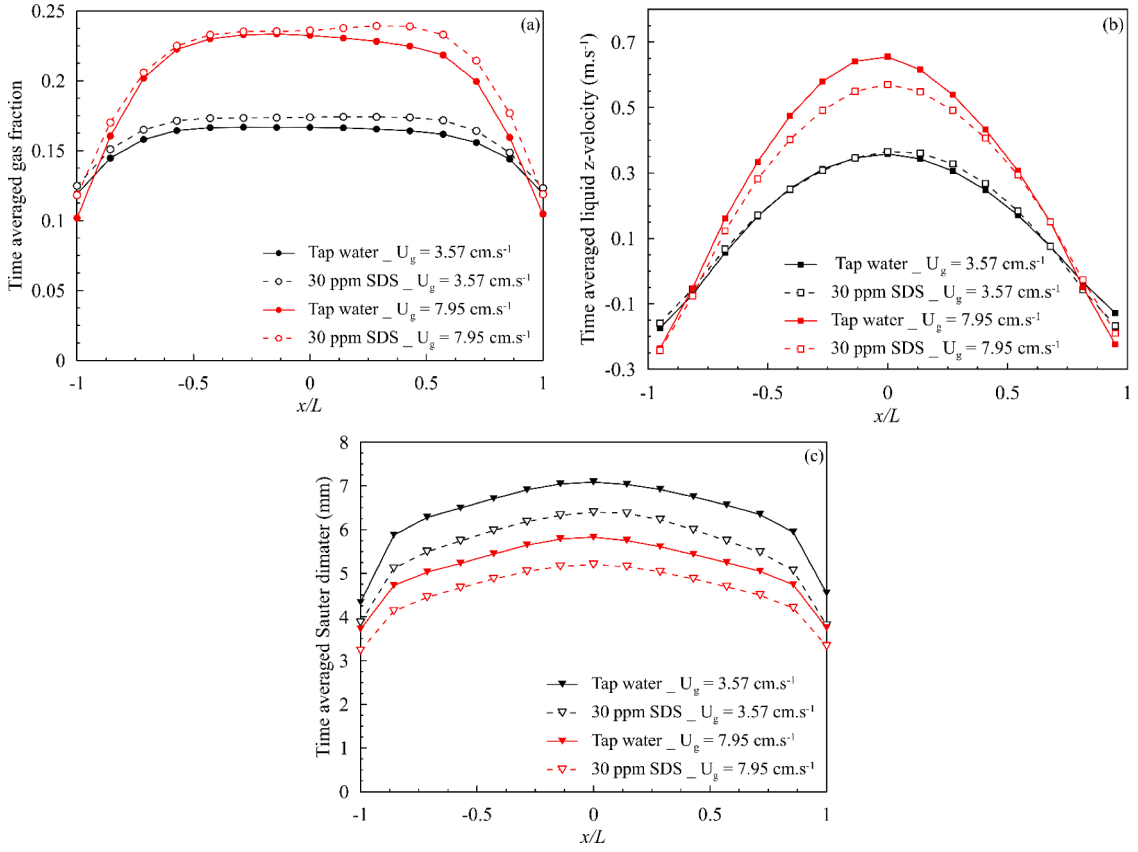

Fig. 9. Impact of contamination. (a) Time-averaged gas fraction, (b) liquid axial velocity, and (c) mean Sauter diameter radial profiles obtained with CFD-PBM simulations at U_g = 3.57 and 7.95 cm.s^{-1} for air-tap water and air-30 ppm of SDS systems.

bubble. The large bubbles formed by coalescence rise faster through the column center with lower residence time, while the small bubbles are preserved within the bubble column which increases the overall gas holdup, as can be observed also in the pictures displayed in Fig.4. Obviously, the gas holdup is influenced by the gas sparger type which is, in this case, a perforated plate that generates primary bubbles with a diameter of about 1 mm. Although they have distinct characteristics and have shown different behaviors, the trend of ε_g versus U_g in SDS aqueous solution exhibits similar behavior in the heterogeneous flow regime compared to the other surfactants that develop foam formation causing a bubble accumulation with a significant increase of the overall gas holdup (Besagni and Inzoli, 2017; Kouzbour et al., 2021). In addition, the global gas holdup in this regime is not affected by the SDS concentration and the gas-liquid interface seems to be saturated by the adsorbed SDS above 5 ppm, this behavior was confirmed by similar studies employing surfactant and antifoaming agents (Koide et al., 1985; Kouzbour et al., 2021). Eventually, through the photographs of bubbles in 30 ppm SDS aqueous solution (Fig. 4), narrow bubble formation at low U_g can be noticed owing to the gas distributor and coalescence inhibition phenomena, while different bubble sizes and foam are observed at high U_g.

CFD-PBM coupled model predictions of the global gas holdup for both tap water and 30 ppm aqueous solutions, in homogeneous and heterogeneous flow regimes, are illustrated in Fig. 6. Notably, it can be

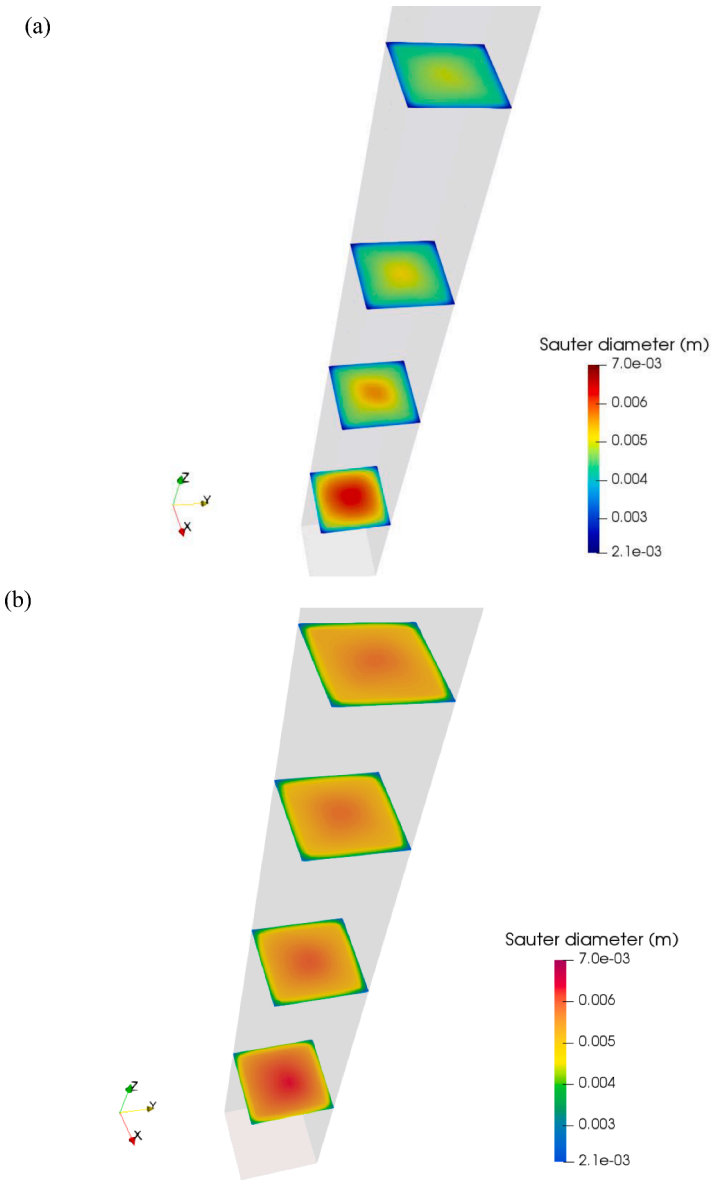

Fig. 10. Contour plots of time-averaged Sauter mean diameter at $U_g = 7.95$ cm.s^{-1} for (a) contaminated water with 30 ppm of SDS and (b) tap water.

seen that the measured and the predicted gas holdup are in reasonable agreement, especially for air- tap water system and for fully homogeneous ($U_g < 4$ cm.s^{-1}) and heterogeneous ($U_g > 9$ cm.s^{-1}) regime. However, the deviation between the measured and the computed gas holdup becomes relatively significant when the liquid phase properties were altered by adding SDS with a concentration of 30 ppm. There could be at least two different explanations for this behavior: it could be due, on one hand, to an inexact modeling of the bubble's coalescence and breakage phenomena, and on the other hand to the estimation of the drag force. However, the fine agreement of the mass transfer coefficient $k_L a_L$, discussed in Section 3.3, which is strongly dependent on the interfacial area, suggests that this deviation is to be related to the estimation of the drag force rather than the bubbles dynamics. Therefore, this behavior may indicate that SDS molecules could have a bigger role in the drag force exerted on the bubbles and this topic could be worthy of investigation for future studies. Besides, in both media, the CFD-PBM coupled model leads to an overestimation of gas holdup in the homogeneous flow regime and its underestimation in the heterogeneous flow regime. Globally, the discrepancy between the measured and calculated values is relatively small in the homogeneous regime. Thus, it can be said that the computational method enables a good prediction of the experimental values while U_g remains low or moderate. Nevertheless, once the transition regime is achieved, the calculations under-predict the ε_g experimental values. This may be due to the bubble size distribution chosen to perform the calculations which does not reflect the chaotic behavior within the bubble column, especially in the heterogeneous regime. Furthermore, the transition between both regimes ($4 < U_g < 8$ cm.s^{-1}) is captured with a relatively larger deviation with respect to the experimental data. Another potential reason behind this deviation could be linked to the modeling aspect and, in particular, to the description of the bubble's coalescence and breakage. Indeed, many kernels developed to describe these phenomena in the PBM equations are specifically designed for a single hydrodynamical regime. Thus, when applied to another regime, their predictive capacity is going to fail. In this study, it was preferred to use a single approach that was not adjusted according to the specific hydrodynamical regime, and therefore, this may contribute to the deviation of the CFD holdup prediction from the experimental measurements, especially in the transition regime. Moreover, the contamination of the liquid phase can also affect the interfacial forces; for instance, the drag coefficient can vary with the

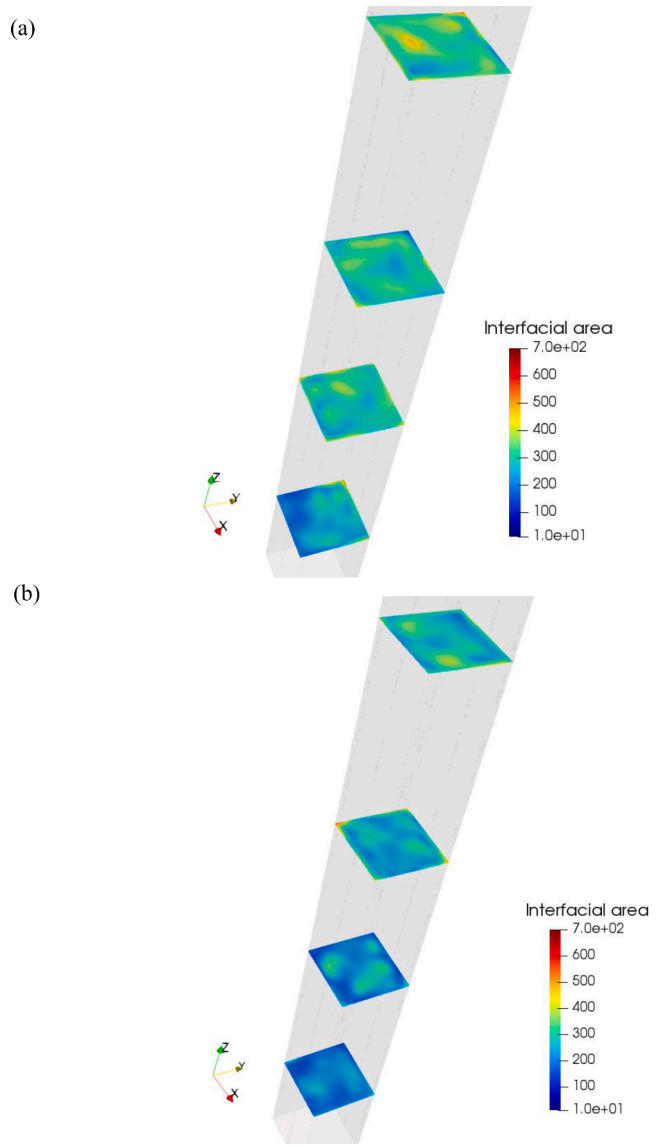

Fig. 11. Instantaneous contour plots of the specific interfacial area at U_g = 7.95 cm.s^{-1} for (a) contaminated water with 30 ppm of SDS and (b) tap water.

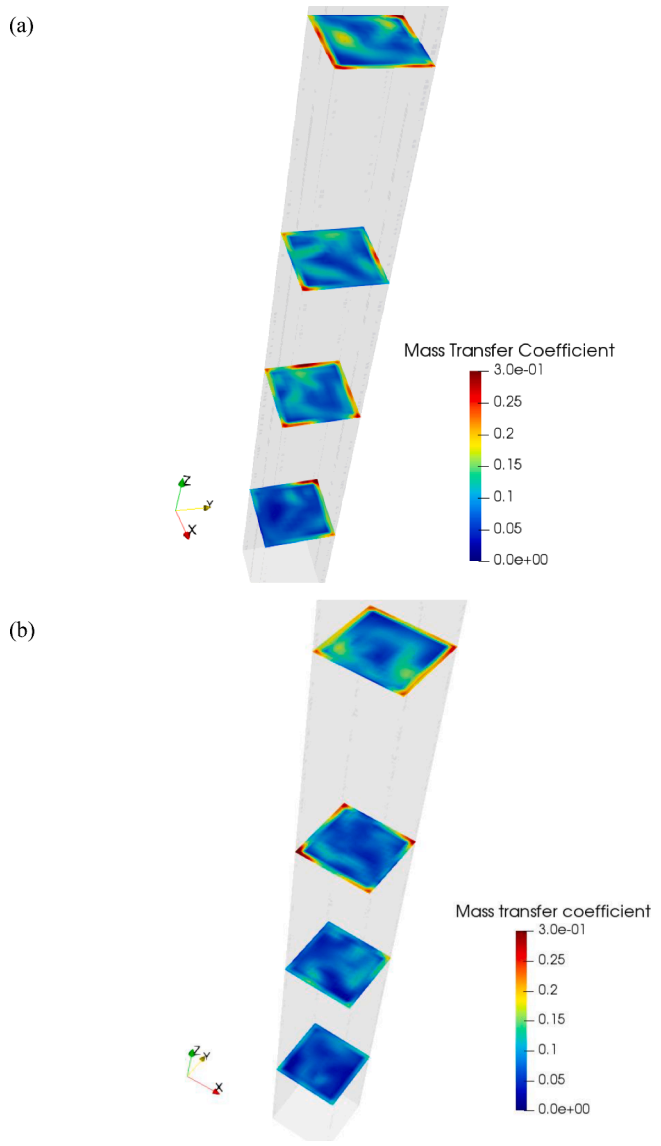

Fig. 12. Instantaneous contour plots of the volumetric mass transfer coefficient $k_L a_L$ at U_g = 7.95 cm.s^{-1} for (a) contaminated water with 30 ppm of SDS and (b) tap water.

degree of water contamination (Tomiyama, 1998), and subsequently impact the global gas holdup. For these reasons, the modeling of such flow behavior requires further development and improvements by deeply studying the relationship between surfactant contamination and interfacial forces.

Snapshots of the flow structures are displayed in Fig. 7. This figure provides and compares instantaneous ε_g and photographs of bubbles distribution at different superficial gas velocities (U_g = 1.19 cm.s^{-1}, 4.90 cm.s^{-1}, and 7.95 cm.s^{-1}) in tap water and 30 ppm SDS aqueous solution. At low gas velocity, the effect of SDS on the bubble distribution is insignificant and the bubble size distribution is narrow. Besides, Small bubbles are uniformly dispersed with minor bubble-bubble interaction within the column as can be noticed in Figs. 7a and b. Conversely, at high gas flow rates, the liquid phase is highly turbulent, and the foaming becomes more prominent in water-SDS solutions than in tap water. The CFD-PBM coupled model and photographs reveal repeatedly that bubbles moving towards the center of the column cause an increase in the liquid average vertical velocity and gas holdup.

The radial profiles of the simulated time-averaged ε_g in the middle of the column are displayed in Fig. 8. According to this figure, the radial profiles of the simulated time-averaged ε_g in the middle of the column are more uniform in the center at low U_g, and become nearly parabolic in the heterogeneous flow regime with a slight increase in the water-SDS solution caused by the presence of small bubbles in the core and close to the walls. This is related to the high density of small bubbles generated by the distributor and preserved within the column as can be observed in Fig. 9. Indeed, the decrease in bubble size is mainly due to the lower surface tension caused by the accumulation of surfactant molecules at the gas-liquid interface and a reduction in the drag interfacial force (Camarasa et al., 1999; McClure et al., 2015). Meanwhile, the increase in the liquid velocity may be attributed to the enhancement of turbulence intensity which induced bubble breakup and, consequently, the decline in the mean bubble size.

3.2. SDS effects on the bubble size

Simulations are then performed to examine the combined effect of superficial gas velocity and surfactant on the bubble size. Fig. 9c depicts the radial distribution of Sauter mean bubble diameter for 30 ppm SDS aqueous solution. The predicted values fall in the range of $4-7$ mm and $3-6$ mm for tap water and 30 ppm SDS aqueous solution, respectively.

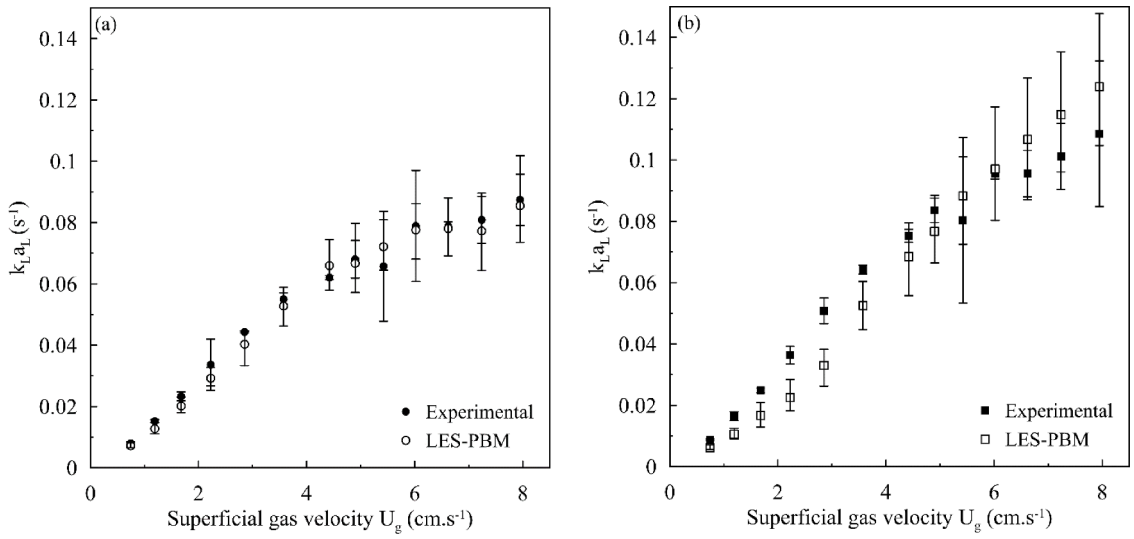

Fig. 13. Estimation of the volumetric mass transfer coefficient through CFD-PBM simulations and comparison with experimental measurements for tap water at the (a) bottom and (b) top probes.

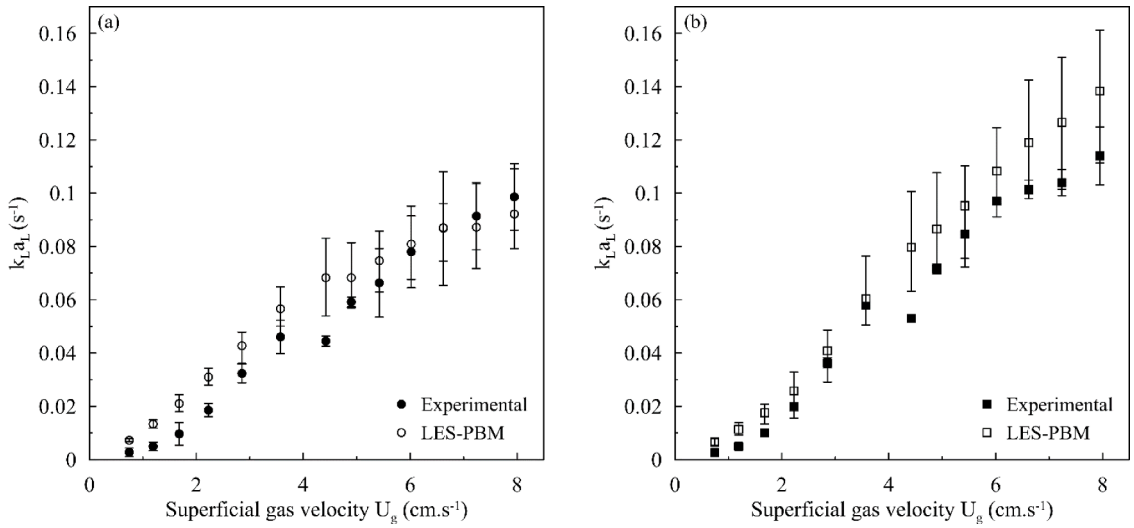

Fig. 14. Estimation of the mass transfer coefficient through CFD-PBM simulations and comparison with experimental measurements for 30 ppm SDS aqueous solution at the (a) bottom (a) and (b) top probes.

Thus, the obtained results are in line with those found by Asgharpour et al. (2010). It should be noted that experimental data related to the contributions of small and large bubbles are unavailable. As expected, in the turbulent-churn flow regime, the bubble size distribution is characterized by larger mean diameters in the core of the column compared to the near-wall regions, and an overall decrease in the mean bubble size clearly occurs with the presence of SDS surfactant. From Fig. 9c, it is noticeable that the evolution of bubble size distribution with the superficial gas velocity is more marked for tap water than for SDS solution, pointing out the important role of the large bubbles and bubble coalescence, at the core region of the column, in determining the flow regime transition and then in the mass transfer. Moreover, Fig. 10 illustrates the instantaneous field of Sauter mean diameter d_{32} along the axial coordinate calculated using the LES-PBM model, for both tap water and 30 ppm SDS aqueous solution. As a result, it appears that the addition of SDS as a contaminant leads to a smaller average bubble size, which is in good accordance with the experimental findings. In fact, SDS molecules are adsorbed preferentially at the bubble-liquid interface, reducing the interface mobility and hence hindering coalescence phenomena. In the computational model, this effect is considered by using the effective surface tension σ correlated to the mixture air-SDS solution used. For the air-tap water system, The Sauter mean diameter increases in the upper part of the column and seems to be approximately uniform as a result of the enhanced bubble coalescence along the column height. This observation was outlined by Jamialahmadi and Muller (1990) and Shimizu et al. (2000).

3.3. Mass transfer coefficient k_L

The local estimation of gas-liquid interfacial a_L, provided by the PBM equations, is crucial when the computation of the liquid side mass transfer coefficient k_La_L is pursued. In this perspective, the calculation of a_L is particularly straightforward as it is related to the moment of the NDF of order two through Eq. (26), which is directly calculated by the QMOM algorithm. Since local measurements are not available, only the predicted results at $U_g = 7.95$ cm.s^{-1} for different cross-sectional areas along the column (Fig. 11). According to Fig. 11, it can be noted that the interfacial area is non-uniform in the radial direction and becomes much more prominent for water-SDS solution because of the larger contribution of small bubbles.

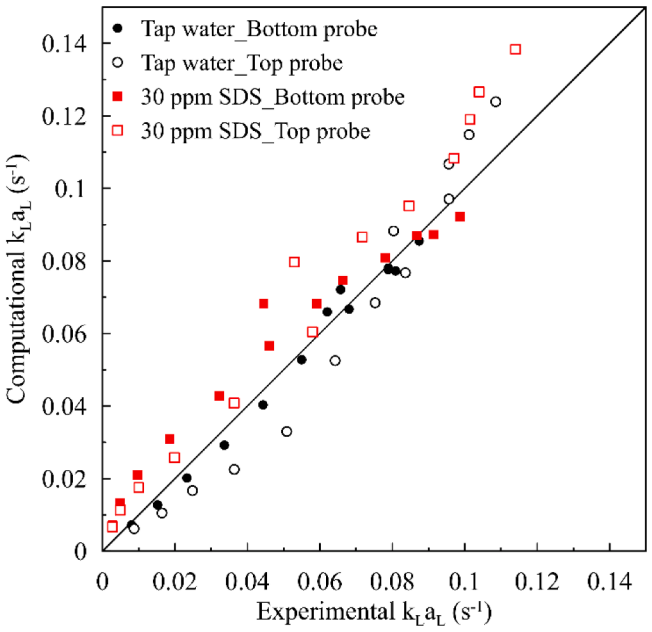

Fig. 15. Parity plot of k_La_L: Comparison of experimental measurements and computational estimations.

Figs. 13–15 exhibit the simulated and measured volumetric mass transfer coefficient in the tap water and SDS aqueous solution as functions of superficial gas velocity. The sampling is computationally performed at the actual positions of the two oximeters, namely the bottom probe (the O_2 probe is placed at 0.11 m above the gas sparger) and the top probe (the O_2 probe is placed at 1.50 m above the gas sparger). Therefore, the coefficient k_La_L calculated by LES-PBM simulations is an average in the domain region corresponding to the experimental measurements. Experimental measurements were first used to validate the proposed LES-PBM coupled computational model. However, it was found that the computational model with the eddy cell model gives good predictions except at the high superficial gas velocity where the flow becomes turbulent, and the level of turbulent energy dissipation required for the cell eddy model needs further research. Also, an additional aspect that stands out is that the measured or calculated mass transfer coefficient at the top probe is generally superior to that obtained by the bottom probe. This can be explained by the fact that in the area close to the gas sparger, the primary gas distribution prevails, which may be quite different from the bubble size distribution in the bulk. Furthermore, this fact is also related to the establishment of the flow patterns, which occur along the axial direction. Indeed, the distance between the sparger and the bottom probe is only 0.11 m, lower than the hydraulic diameter. Consequently, this probe collects samples in a portion of the space where the flow and the resulting agitation are not fully developed yet, which inevitably leads to lower values of k_La_L. In contrast, the top probe retrieves data from a region where the flow is well developed, and the relative mass transfer coefficients are therefore higher.

Fig. 12 shows the evolution of instantaneous and time-averaged values of k_La_L at different cross-sections along the height of the column reactor at $U_g = 7.95$ cm.s^{-1}. It is noted that the local time-averaged volumetric mass transfer coefficient extends from the center to the near wall. The instantaneous results exhibit a non-uniform radial distribution of the mass transfer with an increase in k_La_L at the top center of the column; where most of the gas is accumulated and foaming is developed in the case of the water-SDS solution. This variation is in agreement with the radial fraction distribution displayed in Figs. 10 and 11. Moreover, Fig. 12 indicates that k_La_L values are higher close to the walls of the cross-section. This outcome could be ascribed to the calculation of the turbulence dissipation rate using Eq. (21) coupled with a no-slip condition for the liquid velocity as a boundary condition for the walls. Thus, this could potentially lead to a slight overestimation of the strain rate, the turbulent dissipation rate (Eq. (21)), and ultimately, the coefficient k_L (Eq. (25)) in the immediate proximity of the wall. However, this effect quickly attenuates when approaching the column center.

Based on Figs. 14 and 15, the coefficients k_La_L and k_L augment with increasing U_g. It immediately stands out the growing trend of k_La_L with the superficial gas velocity. This is related to the higher degree of system agitation, which is directly proportional to the velocity of the gas bubbles. Then, this results in an increased surface renewal mobility and, therefore, in an improvement of the mass transfer mechanisms. Nevertheless, k_La_L coefficient in surfactant aqueous solutions is higher compared to that in tap water. Moreover, as mentioned in Subsection 3.2, the addition of SDS to the liquid phase had two opposite effects on k_La_L coefficient: (i) the decrease in k_L due to the lower oxygen diffusivity, and (ii) the increase in a_L owing to the smaller average bubble size. Actually, the latter appears predominant from LES-PBM simulations, once again in line with experimental measurements.

The effect of surfactant addition on the liquid-phase mass transfer coefficient k_L is mainly linked to the modification of hydrodynamic features of the system. Actually, surfactants are adsorbed at the gas-liquid interface, which delays surface flow through the surface tension

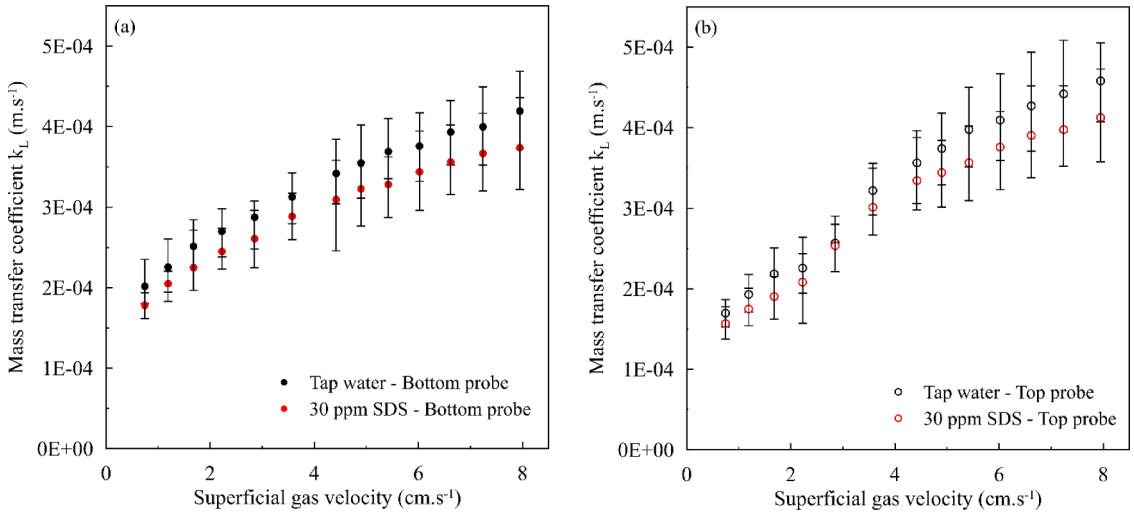

Fig. 16. Numerical estimation of the mass transfer coefficient k_L at (a) the bottom and (b) top probes.

gradient at the interface and therefore induces a decrease in the mass transfer coefficient k_L (Koide et al., 1985; Nock et al., 2016). The complex model dependency of k_L with the local and bubble size was found to be important in the study performed by Vik et al. (2018). Furthermore, as pointed out by Kulkarni et al. (2007), in the established heterogeneous regime, the bubble size distribution and the eddy size distribution have different contributions on k_L. While the former is dependent on the gas distributor and the lower surface tension caused by the surfactant, the eddy size distribution is related to the liquid viscosity and liquid turbulence, as well as to the bubble induced turbulence generated at high superficial gas velocity. Therefore, the true mass transfer coefficient remains difficult to model and measure. The eddy cell model employed here to estimate k_La_L assumes isotropic turbulence, and it is not clear that the contributions to the mass transfer from the small-scale eddy and the turbulence induced by small bubbles due to coalescence rate will be approximated by the weak homogeneous shear turbulence (Shi et al., 2019). However, the parity plot reported in Fig. 16 compared experimental and computational estimation of the mass transfer coefficient, which further confirms the validity of the CFD-PBM model proposed in this study, and, in particular, highlights the accuracy in the k_La_L calculation.

4. Conclusions

This study presents experimental and numerical investigations of the effects of surface-active agents on hydrodynamic characteristics and mass transfer in a square bubble column. The effect of the presence of small quantities of sodium dodecyl sulfate (SDS) in the liquid phase was examined with a special emphasis on its effect on fluid dynamics, bubble size distribution, and mass transfer performances. The CFD simulations were performed by coupling the population balance with an Eulerian-Eulerian large-eddy simulation model. The range of SDS concentrations used for preparing contaminated solutions, varying from 0 ppm to 30 ppm, is extremely low. Hence, the effect of the surfactant occurrence was considered only by reducing the interfacial tension, which was experimentally measured as a function of the SDS concentration. Global measurement data were used to validate the CFD-PBM model and then employed for further local analysis. Experimental data revealed that the presence of the SDS in the liquid phase increased the overall gas holdup to attain 25% at a constant gas velocity in the transition regime because of the inhibited coalescence and the presence of smaller bubbles compared to the air-tap water system. Meanwhile, a further increase in the surfactant concentration to 30 ppm had no additional impact, and the regime flow transition from homogeneous to heterogeneous regimes was delayed to a higher superficial gas velocity of around 5.5 cm.s^{-1}. However, small concentrations of SDS led to an augmentation of the overall mass transfer coefficient at different probe positions only in the heterogeneous flow regime (for $U_G \geq 6$ cm.s^{-1}) due to a larger interfacial area. The impact of the addition of SDS to the liquid phase is dual: on one side, it decreased k_L because the corresponding oxygen diffusivity in water is lower, since the SDS molecules migrate towards the bubble-liquid interface, hindering the O_2 transfer from one phase to the other. On the other side, it also increased due to the inhibition of bubbles coalescence, and therefore, the lower mean bubble size. Among these two effects, the latter is predominant, and thus, k_La_L increased in the contaminated systems.

The predicted and the experimental results show good agreement. The prediction of the gas hold-up is particularly accurate for tap-water, while it decreases its precision in the presence of SDS. This outcome was correlated to a possible effect of the SDS molecules on the drag force and the additional stress caused by the adsorption of molecules on bubble surfaces, which is worthy of investigation for future studies. Further analysis is underway to analyze the impact of the bubble diameter on k_La_L in presence of surfactants at high gas flow rates as well. On the other hand, the implementation of a PBM model allowed the assessment of the bubble size distribution and contributed to the prediction of the local flow pattern. However, the most relevant contribution of this application is the correct estimation of the bubbles interface area, and therefore, of k_La_L. In fact, the proposed model showed its considerable ability to quantify the oxygen mass transfer mechanism with particularly high precision, as suggested by the comparison with experimental data. Numerical predictions of the global gas holdup displayed in Fig. 6, as well as the foam formation shown in Fig. 4, are still being improved by analyzing different turbulence models and coalescence and breakup kernels in the CFD-PBM coupled model, to account for adequate definitions of the population balance for the dispersed phase and the turbulence in the liquid phase. A specific analysis of experimental results would be also of great help.

CRediT author statements

Sanaa Kouzbour: Experimental measurements, Investigation, Results interpretations, Writing – review & editing.

Francesco Maniscalco: Numerical simulations, Post-processing data and results, interpretations, Writing – review & editing.

Antonio Buffo: Numerical simulations, interpretations, Writing – review & editing.

Marco Vanni: Numerical simulations, interpretations, Writing – review & editing.

F. Xavier Grau: Numerical simulations, interpretations, Writing – review & editing.

Gourich Bouchaib: Experimental measurements, Conceptualization, Results interpretations, Writing – review & editing.

Youssef Stiriba: Conceptualization, Numerical simulations, Software, interpretations, Writing – review & editing.

Declaration of Competing Interest

The authors declare that they have no known competing financial interests or personal relationships that could have appeared to influence the work reported in this paper.

Data availability

Data will be made available on request.

Acknowledgments

The authors would like to express their deep appreciation and gratitude for the support of this study provided by the National Center for Scientific and Technological Research (CNRST, Morocco) and by financial grants from the Moroccan Ministry of Higher Education, Scientific Research and Executive Training, High School of Technology (ESTC) and Hassan II University of Casablanca (UH2C). We are also grateful to the Common Infrastructure for National Cohorts in Europe, Canada, and Africa (CINECA) for providing the computational resources through the Italian SuperComputing Resource Allocation – ISCRA (https://www.hpc.cineca.it).

References

Ahmia, A.C., Idouhar, M., Wongwailikit, K., Dietrich, N., Hébrard, G., 2019. Impact of cellulose and surfactants on mass transfer of bubble columns. Chem. Eng. Technol. 42, 2465–2475. https://doi.org/10.1002/ceat.201800620.

Alves, S.S., Orvalho, S.P., Vasconcelos, J.M.T., 2005. Effect of bubble contamination on rise velocity and mass transfer. Chem. Eng. Sci. 60, 1–9. https://doi.org/10.1016/j.ces.2004.07.053.

Aoki, J., Hayashi, K., Hosokawa, S., Tomiyama, A., 2015. Effects of surfactants on mass transfer from single carbon dioxide bubbles in vertical pipes. Chem. Eng. Technol. 38, 1955–1964. https://doi.org/10.1002/ceat.201500063.

Asgharpour, M., Mehrnia, M.R., Mostoufi, N., 2010. Effect of surface contaminants on oxygen transfer in bubble column reactors. Biochem. Eng. J. 49, 351–360. https://doi.org/10.1016/j.bej.2010.01.010.

Aubin, J., Ferrando, M., Jiricny, V., 2010. Current methods for characterising mixing and flow in microchannels. Chem. Eng. Sci. 65, 2065–2093. https://doi.org/10.1016/j.ces.2009.12.001.

Besagni, G., Gallazzini, L., Inzoli, F., 2019. On the scale-up criteria for bubble columns. Petroleum 5, 114–122. https://doi.org/10.1016/j.petlm.2017.12.005. SI: Experimental & Numerical Study of Multiphase Flow Phenomena and Models in Oil & Gas Industry.

Besagni, G., Inzoli, F., 2017. The effect of liquid phase properties on bubble column fluid dynamics: gas holdup, flow regime transition, bubble size distributions and shapes, interfacial areas and foaming phenomena. Chem. Eng. Sci. 170, 270–296. https://doi.org/10.1016/j.ces.2017.03.043.

Camarasa, E., Vial, C., Poncin, S., Wild, G., Midoux, N., Bouillard, J., 1999. Influence of coalescence behaviour of the liquid and of gas sparging on hydrodynamics and bubble characteristics in a bubble column. Chem. Eng. Process. Process Intensif. 38, 329–344. https://doi.org/10.1016/S0255-2701(99)00024-0.

Clift, R., Grace, J.R., Weber, M.E., 2005. Bubbles, drops, and particles. Courier Corporation.

Coulaloglou, C.A., Tavlarides, L.L., 1977. Description of interaction processes in agitated liquid-liquid dispersions. Chem. Eng. Sci. 32, 1289–1297. https://doi.org/10.1016/0009-2509(77)85023-9.

Cuenot, B., Magnaudet, J., Spennato, B., 1997. The effects of slightly soluble surfactants on the flow around a spherical bubble. J. Fluid Mech. 339, 25–53. https://doi.org/10.1017/S0022112097005053.

Danckwerts, P.V., 1951. Significance of liquid-film coefficients in gas absorption. Ind. Eng. Chem. 43, 1460–1467. https://doi.org/10.1021/ie50498a055.

Dani, A., Cockx, A., Guiraud, P., 2006. Direct numerical simulation of mass transfer from spherical bubbles: the effect of interface contamination at low Reynolds numbers. Int. J. Chem. React. Eng. 4 https://doi.org/10.2202/1542-6580.1304.

Falzone, S., Buffo, A., Vanni, M., Marchisio, D.L., 2018. Chapter three - simulation of turbulent coalescence and breakage of bubbles and droplets in the presence of surfactants, salts, and contaminants. In: Parente, A., De Wilde, J. (Eds.), Advances in Chemical Engineering, Bridging Scales in Modelling and Simulation of Non-Reacting and Reacting Flows. Part I. Academic Press, pp. 125–188. https://doi.org/10.1016/bs.ache.2018.01.002.

Fard, M.G., Striba, Y., Gourich, B., Vial, C., Grau, F.X., 2020a. Euler-Euler large eddy simulations of the gas–liquid flow in a cylindrical bubble column. Nucl. Eng. Des. 369, 110823 https://doi.org/10.1016/j.nucengdes.2020.110823.

Fard, M.G., Vernet, A., Striba, Y., Grau, X., 2020b. Transient large-scale two-phase flow structures in a 3D bubble column reactor. Int. J. Multiph. Flow 127, 103236. https://doi.org/10.1016/j.ijmultiphaseflow.2020.103236.

García-Abuín, A., Gómez-Díaz, D., Navaza, J.M., Sanjurjo, B., 2010. Effect of surfactant nature upon absorption in a bubble column. Chem. Eng. Sci. 65, 4484–4490. https://doi.org/10.1016/j.ces.2010.04.009.

Gemello, L., Cappello, V., Augier, F., Marchisio, D., Plais, C., 2018. CFD-based scale-up of hydrodynamics and mixing in bubble columns. Chem. Eng. Res. Des. 136, 846–858. https://doi.org/10.1016/j.cherd.2018.06.026.

Gemello, L., Plais, C., Augier, F., Marchisio, D.L., 2019. Population balance modelling of bubble columns under the heterogeneous flow regime. Chem. Eng. J. 372, 590–604. https://doi.org/10.1016/j.cej.2019.04.109.

Gómez-Díaz, D., Gomes, N., Teixeira, J.A., Belo, I., 2009. Oxygen mass transfer to emulsions in a bubble column contactor. Chem. Eng. J. 152, 354–360. https://doi.org/10.1016/j.cej.2009.04.059.

Gourich, B., Vial, Ch., Soulami, M.B., Zoulalian, A., Ziyad, M., 2008. Comparison of hydrodynamic and mass transfer performances of an emulsion loop-venturi reactor in cocurrent downflow and upflow configurations. Chem. Eng. J. 140, 439–447. https://doi.org/10.1016/j.cej.2007.11.011.

Haghnegahdar, M., Boden, S., Hampel, U., 2016. Investigation of surfactant effect on the bubble shape and mass transfer in a milli-channel using high-resolution microfocus X-ray imaging. Int. J. Multiph. Flow 87, 184–196. https://doi.org/10.1016/j.ijmultiphaseflow.2016.09.010.

Hébrard, G., Zeng, J., Loubière, K., 2009. Effect of surfactants on liquid side mass transfer coefficients: a new insight. Chem. Eng. J. 148, 132–138. https://doi.org/10.1016/j.cej.2008.08.027.

Higbie, R., 1935. The rate of absorption of a pure gas into a still liquid during short periods of exposure. Trans. AIChE 31, 365–389.

Jamialahmadi, M., Muller, Steinhagen H., 1990. A study of gas hold-up in two and three-phase bubble columns. In: Chemeca 90: The Eighteenth Australasian Chemical Engineering Conference; Processing Pacific Resources. Presented at the Chemeca 90: The Eighteenth Australasian Chemical Engineering Conference; Processing Pacific Resources. Chemical Engineering Group (New Zealand, Auckland, N.Z, pp. 1188–1195. https://doi.org/10.3316/informit.847389673627923.

Jamnongwong, M., Loubière, K., Dietrich, N., Hébrard, G., 2010. Experimental study of oxygen diffusion coefficients in clean water containing salt, glucose or surfactant: consequences on the liquid-side mass transfer coefficients. Chem. Eng. J. 165, 758–768. https://doi.org/10.1016/j.cej.2010.09.040.

Jia, X., Hu, W., Yuan, X., Yu, K., 2015. Effect of surfactant type on interfacial area and liquid mass transfer for CO2 absorption in a bubble column. Chin. J. Chem. Eng. 23, 476–481. https://doi.org/10.1016/j.cjche.2014.11.027.

Koide, K., Yamazoe, S., Harada, S., 1985. Effects of surface-active substances on gas holdup and gas-liquid mass transfer in bubble column. J. Chem. Eng. Jpn. 18, 287–292. https://doi.org/10.1252/jcej.18.287.

Kouzbour, S., Gourich, B., Striba, Y., Vial, C., Gros, F., Sotudeh-Gharebagh, R., 2021. Experimental analysis of the effects of liquid phase surface tension on the hydrodynamics and mass transfer in a square bubble column. Int. J. Heat Mass Transf. 170, 121009 https://doi.org/10.1016/j.ijheatmasstransfer.2021.121009.

Koynov, A., Khinast, J.G., Tryggvason, G., 2005. Mass transfer and chemical reactions in bubble swarms with dynamic interfaces. AIChE J. 51, 2786–2800. https://doi.org/10.1002/aic.10529.

Koynov, A., Tryggvason, G., Schlüter, M., Khinast, J.G., 2006. Mass transfer and chemical reactions in reactive deformable bubble swarms. Appl. Phys. Lett. 88, 134102 https://doi.org/10.1063/1.2188054.

Kulkarni, A.A., Ekambara, K., Joshi, J.B., 2007. On the development of flow pattern in a bubble column reactor: experiments and CFD. Chem. Eng. Sci. 62, 1049–1072. https://doi.org/10.1016/j.ces.2006.10.011.

Laakkonen, M., Alopaeus, V., Aittamaa, J., 2006. Validation of bubble breakage, coalescence and mass transfer models for gas–liquid dispersion in agitated vessel. Chem. Eng. Sci., Advances in population balance modelling 61, 218–228. https://doi.org/10.1016/j.ces.2004.11.066.

Laakkonen, M., Moilanen, P., Alopaeus, V., Aittamaa, J., 2007. Modelling local bubble size distributions in agitated vessels. Chem. Eng. Sci. 62, 721–740. https://doi.org/10.1016/j.ces.2006.10.006.

Lamont, J.C., Scott, D.S., 1970. An eddy cell model of mass transfer into the surface of a turbulent liquid. AIChE J. 16, 513–519. https://doi.org/10.1002/aic.690160403.

Lebrun, G., Benaissa, S., Le Men, C., Pimienta, V., Hébrard, G., Dietrich, N., 2022. Effect of surfactant lengths on gas-liquid oxygen mass transfer from a single rising bubble. Chem. Eng. Sci. 247, 117102 https://doi.org/10.1016/j.ces.2021.117102.

Lehr, F., Millies, M., Mewes, D., 2002. Bubble-Size distributions and flow fields in bubble columns. AIChE J. 48, 2426–2443. https://doi.org/10.1002/aic.690481103.

Lopez de Bertodano, M., Lahey, R.T., Jones, O.C., 1994. Phase distribution in bubbly two-phase flow in vertical ducts. Int. J. Multiph. Flow 20, 805–818. https://doi.org/10.1016/0301-9322(94)90095-7.

Maniscalco, F., Buffo, A., Marchisio, D., Vanni, M., 2021. Numerical simulation of bubble columns: LES turbulence model and interphase forces blending approach. Chem. Eng. Res. Des. 173, 1–14. https://doi.org/10.1016/j.cherd.2021.06.024.

Marchisio, D.L., Dennis Vigil, R., O Fox, R., 2003a. Implementation of the quadrature method of moments in CFD codes for aggregation–breakage problems. Chem. Eng. Sci. 58, 3337–3351. https://doi.org/10.1016/S0009-2509(03)00211-2.

Marchisio, D.L., Vigil, R.D., Fox, R.O., 2003b. Quadrature method of moments for aggregation–breakage processes. J. Colloid Interface Sci. 258, 322–334. https://doi.org/10.1016/S0021-9797(02)00054-1.

McClure, D.D., Lee, A.C., Kavanagh, J.M., Fletcher, D.F., Barton, G.W., 2015. Impact of surfactant addition on oxygen mass transfer in a bubble column. Chem. Eng. Technol. 38, 44–52. https://doi.org/10.1002/ceat.201400403.

Milelli, M., Smith, B.L., Lakehal, D., 2001. Large-Eddy simulation of turbulent shear flows laden with bubbles, in: Geurts, B.J., Friedrich, R., Métais, O. (Eds.), Direct and Large-Eddy Simulation IV, ERCOFTAC Series. Springer Netherlands, Dordrecht, pp. 461–470. https://doi.org/10.1007/978-94-017-1263-7_55.

Muniz, M., Sommerfeld, M., 2020. On the force competition in bubble columns: a numerical study. Int. J. Multiph. Flow 128, 103256. https://doi.org/10.1016/j.ijmultiphaseflow.2020.103256.

Nekoeian, S., Aghajani, M., Alavi, S.M., Sotoudeh, F., 2021. Effect of surfactants on mass transfer coefficients in bubble column contactors: an interpretative critical review study. Rev. Chem. Eng. 37, 585–617. https://doi.org/10.1515/revce-2018-0089.

Nock, W.J., Heaven, S., Banks, C.J., 2016. Mass transfer and gas–liquid interface properties of single CO2 bubbles rising in tap water. Chem. Eng. Sci. 140, 171–178. https://doi.org/10.1016/j.ces.2015.10.001.

Painmanakul, P., Loubière, K., Hébrard, G., Mietton-Peuchot, M., Roustan, M., 2005. Effect of surfactants on liquid-side mass transfer coefficients. Chem. Eng. Sci. 60, 6480–6491. https://doi.org/10.1016/j.ces.2005.04.053.

Palmer, M., Hatley, H., 2018. The role of surfactants in wastewater treatment: impact, removal and future techniques: a critical review. Water Res. 147, 60–72. https://doi.org/10.1016/j.watres.2018.09.039.

Salmani, M.H., Davoodi, M., Ehrampoush, M.H., Ghaneian, M.T., Fallahzadah, M.H., 2013. Removal of cadmium (II) from simulated wastewater by ion flotation technique. Iran. J. Environ. Health Sci. Eng. 10, 16. https://doi.org/10.1186/1735-2746-10-16.

Sardeing, R., Painmanakul, P., Hébrard, G., 2006. Effect of surfactants on liquid-side mass transfer coefficients in gas–liquid systems: a first step to modeling. Chem. Eng. Sci. 61, 6249–6260. https://doi.org/10.1016/j.ces.2006.05.051.

Sato, Y., Sekoguchi, K., 1975. Liquid velocity distribution in two-phase bubble flow. Int. J. Multiph. Flow 2, 79–95. https://doi.org/10.1016/0301-9322(75)90030-0.

Shah, Y.T., Kelkar, B.G., Godbole, S.P., Deckwer, W.-D., 1982. Design parameters estimations for bubble column reactors. AIChE J. 28, 353–379. https://doi.org/10.1002/aic.690280302.

Shamshirband, S., Babanezhad, M., Mosavi, A., Nabipour, N., Hajnal, E., Nadai, L., Chau, K.-W., 2020. Prediction of flow characteristics in the bubble column reactor by the artificial pheromone-based communication of biological ants. Eng. Appl. Comput. Fluid Mech. 14, 367–378. https://doi.org/10.1080/19942060.2020.1715842.

Shi, W., Yang, X., Sommerfeld, M., Yang, J., Cai, X., Li, G., Zong, Y., 2019. Modelling of mass transfer for gas-liquid two-phase flow in bubble column reactor with a bubble breakage model considering bubble-induced turbulence. Chem. Eng. J. 371, 470–485. https://doi.org/10.1016/j.cej.2019.04.047.

Shiea, M., Mostoufi, N., Sotudeh-Gharebagh, R., 2013. Comprehensive study of regime transitions throughout a bubble column using resistivity probe. Chem. Eng. Sci. 100, 15–22. https://doi.org/10.1016/j.ces.2013.01.047.

Shimizu, K., Takada, S., Minekawa, K., Kawase, Y., 2000. Phenomenological model for bubble column reactors: prediction of gas hold-ups and volumetric mass transfer coefficients. Chem. Eng. J. 78, 21–28. https://doi.org/10.1016/S1385-8947(99)00165-5.

Simonnet, M., Gentric, C., Olmos, E., Midoux, N., 2008. CFD simulation of the flow field in a bubble column reactor: importance of the drag force formulation to describe regime transitions. Chem. Eng. Process. Process Intensif. 47, 1726–1737. https://doi.org/10.1016/j.cep.2007.08.015.

Smagorinsky, J., 1963. General circulation experiments with the primitive equations: I. The basic equations. Mon. Weather Rev. 91, 99–164. https://doi.org/10.1175/1520-0493(1963)091<0099:GCEWTP>2.3.CO;2.

Sovová, H., 1981. Breakage and coalescence of drops in a batch stirred vessel—II comparison of model and experiments. Chem. Eng. Sci. 36, 1567–1573. https://doi.org/10.1016/0009-2509(81)85117-2.

Takagi, S., Matsumoto, Y., 2011. Surfactant effects on bubble motion and bubbly flows. Annu. Rev. Fluid Mech. 43, 615–636. https://doi.org/10.1146/annurev-fluid-122109-160756.

Tomiyama, A., 1998. Struggle with computational bubble dynamics. Multiph. Sci. Technol. 10, 369–405. https://doi.org/10.1615/MultScienTechn.v10.i4.40.

Tomiyama, A., Kataoka, I., Zun, I., Sakaguchi, T., 1998. Drag coefficients of single bubbles under normal and micro gravity conditions. JSME Int. J. Ser. B 41, 472–479. https://doi.org/10.1299/jsmeb.41.472.

Tomiyama, A., Tamai, H., Zun, I., Hosokawa, S., 2002. Transverse migration of single bubbles in simple shear flows. Chem. Eng. Sci. 57, 1849–1858. https://doi.org/10.1016/S0009-2509(02)00085-4.

Vial, C., Camarasa, E., Poncin, S., Wild, G., Midoux, N., Bouillard, J., 2000. Study of hydrodynamic behaviour in bubble columns and external loop airlift reactors through analysis of pressure fluctuations. Chem. Eng. Sci. 55, 2957–2973. https://doi.org/10.1016/S0009-2509(99)00551-5.

Vik, C.B., Solsvik, J., Hillestad, M., Jakobsen, H.A., 2018. A multifluid-PBE model for simulation of mass transfer limited processes operated in bubble columns. Comput. Chem. Eng. 110, 115–139. https://doi.org/10.1016/j.compchemeng.2017.11.023.

Wheeler, J.C., 1974. Modified moments and Gaussian quadratures. Rocky Mt. J. Math. 4, 287–296.

Yang, N., Wu, Z., Chen, J., Wang, Y., Li, J., 2011. Multi-scale analysis of gas–liquid interaction and CFD simulation of gas–liquid flow in bubble columns. Chem. Eng. Sci. 66, 3212–3222. https://doi.org/10.1016/j.ces.2011.02.029.

Zhang, D., Deen, N.G., Kuipers, J.A.M., 2006. Numerical simulation of the dynamic flow behavior in a bubble column: a study of closures for turbulence and interface forces. Chem. Eng. Sci. 61, 7593–7608. https://doi.org/10.1016/j.ces.2006.08.053.

Ziaei-Halimejani, H., Kouzbour, S., Zarghami, R., Sotudeh-Gharebagh, R., Gourich, B., Mostoufi, N., Stiriba, Y., 2021. Monitoring of the bubble columns hydrodynamics by recurrence quantification data analysis. Chem. Eng. Res. Des. 171, 100–110. https://doi.org/10.1016/j.cherd.2021.05.002.